

NUCLEAR DATA AND MEASUREMENTS SERIES

ANL/NDM-127

**Fast-Neutron Interaction with
Collective Cadmium Nuclei**

by

A.B. Smith and P.T. Guenther

November 1992

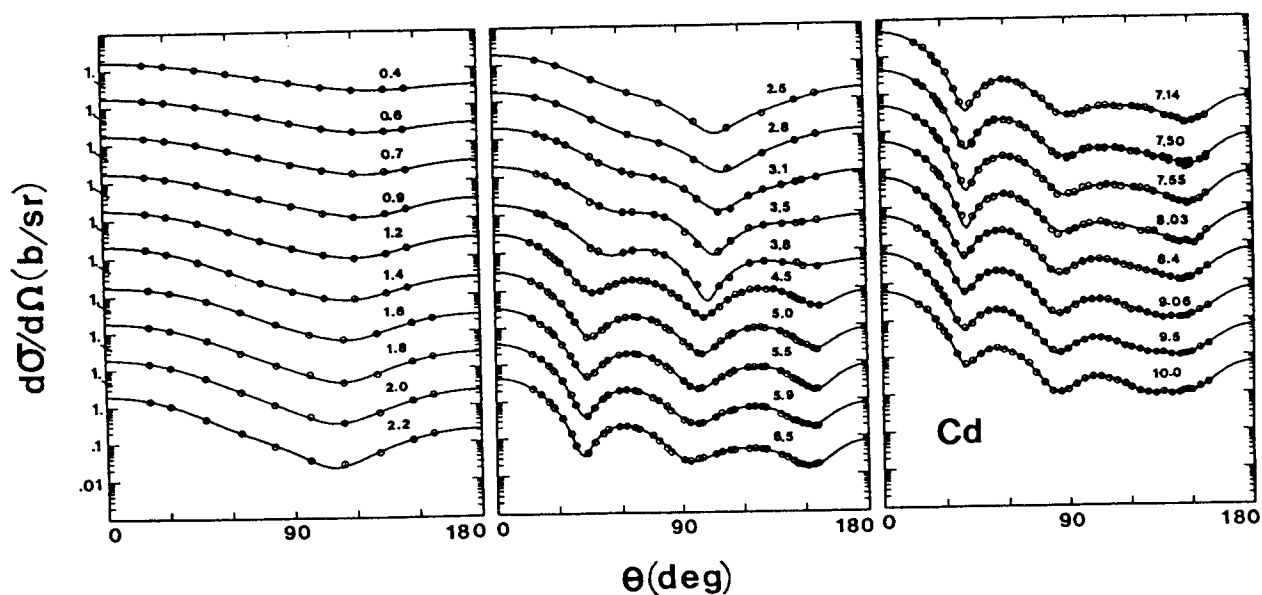
**ARGONNE NATIONAL LABORATORY,
ARGONNE, ILLINOIS 60439, U.S.A.**

NUCLEAR DATA AND MEASUREMENTS SERIES

ANL/NDM-127

FAST-NEUTRON INTERACTION WITH COLLECTIVE
CADMIUM NUCLEI

A. B. Smith and P. T. Guenther
November 1992



ARGONNE NATIONAL LABORATORY, ARGONNE, ILLINOIS

Operated by THE UNIVERSITY OF CHICAGO

for the U. S. DEPARTMENT OF ENERGY

under Contract W-31-109-Eng-38

Argonne National Laboratory, with facilities in the states of Illinois and Idaho, is owned by the United States government, and operated by The University of Chicago under the provisions of a contract with the Department of Energy.

DISCLAIMER

This report was prepared as an account of work sponsored by an agency of the United States Government. Neither the United States Government nor any agency thereof, nor any of their employees, makes any warranty, express or implied, or assumes any legal liability or responsibility for the accuracy, completeness, or usefulness of any information, apparatus, product, or process disclosed, or represents that its use would not infringe privately owned rights. Reference herein to any specific commercial product, process, or service by trade name, trademark, manufacturer, or otherwise, does not necessarily constitute or imply its endorsement, recommendation, or favoring by the United States Government or any agency thereof. The views and opinions of authors expressed herein do not necessarily state or reflect those of the United States Government or any agency thereof.

Reproduced from the best available copy.

Available to DOE and DOE contractors from the
Office of Scientific and Technical Information
P.O. Box 62
Oak Ridge, TN 37831
Prices available from (615) 576-8401

Available to the public from the
National Technical Information Service
U.S. Department of Commerce
5285 Port Royal Road
Springfield, VA 22161

ANL/NDM-127

FAST-NEUTRON INTERACTION WITH COLLECTIVE CADMIUM NUCLEI

by

A. B. Smith and P. T. Guenther

Keywords:

Measured $d\sigma/d\Omega_{el}$ and $d\sigma/d\Omega_{inel}$ for ≤ 10.0 MeV neutrons incident on cadmium. Physical interpretation. Optical statistical, dispersive optical, coupled channels models.

Engineering Physics Division
Argonne National Laboratory
9700 South Cass Avenue
Argonne, Illinois 60439
U. S. A

PRIOR ISSUES IN THE ANL/NDM SERIES

A listing of recent issues in this series is given below. Issues and/or titles prior to ANL/NDM-100 can be obtained from the National Technical Information Service, U. S. Department of Commerce, 5285 Port Royal Road, Springfield, VA 22161, or by contacting one of the authors of this report at the following address:-

Engineering Physics Division
Argonne National Laboratory
9700 South Cass Avenue
Argonne, IL 60439
USA

- A.B. SMITH, P.T. GUENTHER AND R.D. LAWSON
The Energy Dependence of the Optical-Model Potential for Fast-Neutron Scattering From Bismuth
ANL/NDM-100 (1987)
- A.B. SMITH, P.T. GUENTHER, J.F. WHALEN AND R.D. LAWSON
Cobalt, Fast Neutrons and Physical Models
ANL/NDM-101 (1987)
- D.L. SMITH
Investigation of the Influence of the Neutron Spectrum in Determinations of Integral Neutron Cross-Section Ratios
ANL/NDM-102 (1987)
- A.B. SMITH, P. GUENTHER and B. MICKLICH
Spectrum of Neutrons Emitted From a Thick Beryllium Target Bombarded With 7 MeV Deuterons
ANL/NDM-103 (1988)
- L.P. GERALDO and D.L. SMITH
Some Thoughts on Positive Definiteness in the Consideration of Nuclear Data Covariance Matrices
ANL/NDM-104 (1988)
- A. B. SMITH, D.L. SMITH, P.T. GUENTHER, J.W. MEADOWS, R. D. LAWSON, R.J. HOWERTON, and T. DJEMIL
Neutronic Evaluated Nuclear Data File for Vanadium
ANL/NDM-105 (1988)
- A.B. SMITH, P.T. GUENTHER, AND R.D. LAWSON
Fast-Neutron Elastic Scattering from Elemental Vanadium
ANL/NDM-106 (1988)
- P.T. GUENTHER, R.D. LAWSON, M. SUGIMOTO, A.B. SMITH, AND D.L. SMITH
An Evaluated Neutronic Data File for Elemental Cobalt
ANL/NDM-107 (1988)

- M. SUGIMOTO, P.T. GUENTHER, J.E. LYNN, A.B. SMITH, AND J.F. WHALEN
Some Comments on the Interaction of Fast-Neutrons with Beryllium
 ANL/NDM-108 (1988)
- P.T. GUENTHER, R.D. LAWSON, J.W. MEADOWS, A.B. SMITH, D.L. SMITH, AND
 M. SUGIMOTO
An Evaluated Neutronic Data File for Bismuth
 ANL/NDM-109 (March 1989)
- D.L. SMITH AND L.P. GERALDO
A Vector Model for Error Propagation
 ANL/NDM-110 (March 1989)
- J.E. LYNN
Fifty Years of Nuclear Fission
 ANL/NDM-111 (June 1989)
- S. CHIBA, P.T. GUENTHER, AND A.B. SMITH
*Some Remarks on the Neutron Elastic- and Inelastic-Scattering
 Cross Sections of Palladium*
 ANL/NDM-112 (May 1989)
- J.E. LYNN
Resonance Effects in Neutron Scattering Lengths
 ANL/NDM-113 (June 1989)
- A.B. SMITH, R.D. LAWSON, AND P.T. GUENTHER
*Ambiguities in the Elastic Scattering of 8 MeV neutrons from
 Adjacent Nuclei*
 ANL/NDM-114, January 1990
- A.B. SMITH, S. CHIBA, D.L. SMITH, J.W. MEADOWS, P.T. GUENTHER, R.D.
 LAWSON, AND R.J. HOWERTON
Evaluated Neutronic File for Indium
 ANL/NDM-115, January 1990
- S. CHIBA, P.T. GUENTHER, R.D. LAWSON, AND A.B. SMITH
*Neutron Scattering from Elemental Indium, the Optical Model, and
 the Bound-State Potential*
 ANL/NDM-116, June 1990
- D.L. SMITH AND L.P. GERALDO
*An Evaluation of the Nb-93(n,n')Nb-93m Dosimeter Reaction for
 ENDF/B-VI*
 ANL/NDM-117 (November 1990)
- J.W. MEADOWS
*Characteristics of the Samples in the FNG Fission Deposit
 Collection*
 ANL/NDM-118 (November 1990)

- S. CHIBA, P.T. GUENTHER, A.B. SMITH, M. SUGIMOTO, AND R.D. LAWSON
Fast-Neutron Interaction with Elemental Zirconium, and the Dispersive Optical Model
ANL/NDM-119, June 1991
- A.B. SMITH, P.T. GUENTHER, J.F. WHALEN, AND S. CHIBA
Fast-neutron Total and Scattering Cross Sections of ^{58}Ni and Nuclear Models
ANL/NDM-120, July 1991
- S. CHIBA AND D.L. SMITH
A Suggested Procedure for Resolving an Anomaly in Least-squares Data Analysis Known as "Peelle's Pertinent Puzzle" and the General Implications for Nuclear Data Evaluation
ANL/NDM-121, September 1991
- D.L. SMITH AND DOMINIQUE FEAUTRIER
Development and Testing of a Deuterium Gas Target Assembly for Neutron Production Via the $\text{H-2}(D,N)\text{HE-3}$ Reaction at a Low-energy Accelerator Facility
ANL/NDM-122, March 1992
- D.L. SMITH AND E.T. CHENG
A Review of Nuclear Data Needs and Their Status for Fusion Reactor Technology with some Suggestions on a Strategy to Satisfy the Requirements
ANL/NDM-123, September 1991
- J.W. MEADOWS
The Thick-Target $^9\text{Be}(d,n)$ Neutron Spectra for Deuteron Energies Between 2.6 and 7.0-MeV
ANL/NDM-124, November 1991
- A.B. SMITH AND P.T. GUENTHER
Fast-Neutron Scattering Near Shell Closures:- Scandium
ANL/NDM-125, August 1992
- A.B. SMITH, J.W. MEADOWS AND R.J. HOWERTON
A Basic Evaluated Neutronic Data File for Elemental Scandium
ANL/NDM-126, September 1992

TABLE OF CONTENTS

Abstract-----	vi
I. Introduction-----	1
II. Experimental Methods-----	2
III. Experimental Results-----	3
IV. Physical Interpretation-----	10
V. Discussion and Summary-----	34
References-----	41

FAST NEUTRON INTERACTION WITH COLLECTIVE CADMIUM NUCLEI

by

A. B. Smith and P. T. Guenther
Argonne National Laboratory
Argonne, Illinois
and
The Physicist's Consultive
Downers Grove, Illinois

ABSTRACT

Differential neutron elastic-scattering cross sections of elemental cadmium are measured from ≈ 1.5 to 10 MeV. From ≈ 1.5 to 3.0 MeV the measurements are made at ≈ 100 keV incident-neutron energy intervals and at 10 scattering angles distributed between $\approx 20^\circ$ and 160° . From 3 to 4 MeV the measurements are made at ≈ 200 keV intervals and at 20 angles. Above 4 MeV the incident-energy interval is ≈ 0.5 MeV with ≥ 40 differential values at each incident energy, distributed between $\approx 18^\circ$ and 160° . Concurrently, differential cross sections for the excitation of observed "levels" at 0.589 ± 0.047 , 1.291 ± 0.066 and 1.839 ± 0.57 MeV are determined, with attention to the direct excitation of the yrast 2^+ levels of the even isotopes ($\approx 75\%$ abundant) and of the $3/2^+$ and $5/2^+$ levels of the odd isotopes ($\approx 25\%$ abundant). Optical-statistical, dispersive-optical and coupled-channels interpretations are carried out and comparisons made with "regional" and "global" parameters. Consideration is given to the fundamental nature of the real potential in the vicinity of the Fermi Surface with implications on the equation of state and the reduced mass, in the context of the dispersive optical model.

I. INTRODUCTION

Approximately sixty years ago, Fermi and co-workers in Rome noted that some elements had very large absorption cross sections for slow neutrons. Prominent of these is cadmium, and the metal has been widely used as a neutron absorber over the intervening years. The first nuclear reactor (CP-1) employed cadmium control rods half a century ago. With this long, wide and prominent application of cadmium in nuclear technology, one would have thought that the neutron cross sections of the prominent isotopes would be well known. Indeed, that is so for near-thermal neutron absorption, but other cross sections at higher energies, that must be dealt with in many applications, are essentially unknown. For example, cadmium elastic neutron scattering, as defined by the national evaluated file system (ENDF/B-VI) [1], is specified to be isotropic at all energies. That is a gross mis-representation at all but the very lowest energies, and one which makes neutronic calculations at higher energies unreliable, if not deceptive. These are significant matters when, for example, dealing with fast-reactor fission-products and fuel-cycle predictions. Clearly, improved understanding of the neutron cross sections of the cadmium isotopes, important to applications, is overdue.

The cadmium isotopes are collective in nature, and it is reasonable to expect considerable direct neutron reactions. It is known that these collective properties are reflected in the conventional optical-statistical models as large mass-dependent absorptions [2]. Moreover, the electro-magnetic properties of cadmium isotopes have been very carefully studied [3], and it is attractive to attempt to correlate the fundamental electro-magnetic properties with the matrix elements governing the inelastic-neutron transitions and thus provide a promising vehicle for the calculation of direct neutron processes. This theoretical approach is described in ref. [4], and the provision of neutron data to support these concepts was a motivation for this experimental study. In addition, primarily as a result of work at this laboratory, systematic trends in the anomalous behavior of the real optical potential near the Fermi energy are emerging, and these are related to the equation of state and to dispersion effects. Improved definition of this behavior, particularly in the context of strong collective nuclei, was sought. Although the cadmium isotopes are not strictly collective vibrators, for simplicity the neutron reaction with them will be modeled assuming that they are one- and two-phonon collective vibrators.

Elemental cadmium consists of the eight isotopes ^{106}Cd (1.25%), ^{108}Cd (0.89%), ^{110}Cd (12.49%), ^{111}Cd (12.80%), ^{112}Cd (24.13%), ^{113}Cd (12.22%), ^{114}Cd (28.73) and ^{116}Cd (7.49%). In the present work, ^{106}Cd and ^{108}Cd were ignored due to their very low natural abundance. ^{116}Cd was also ignored as its abundance is relatively low, and its

excited structure is quite similar to that of ^{114}Cd .

Subsequent sections of this report deal with; II) a very brief description of the experimental methods, III) the experimental results, IV) the physical interpretation, and V) summary discussion and comments. An associated document addresses the evaluated neutronic files of the cadmium isotopes [5].

II. EXPERIMENTAL METHODS

All of the measurements of this work were made using the fast-neutron time-of-flight technique [6], implemented with the Argonne 10-angle detection apparatus [7]. The technique and apparatus have been used at the Argonne National Laboratory for many years, and are extensively described elsewhere [8 - 11]. Therefore, only brief additional remarks, specifically relevant to these particular measurements, are made here.

All of the present measurements used a solid cylindrical sample of elemental cadmium metal, 2 cm in diameter and 2 cm long. The chemical purity of the sample was $> 99\%$. Similar-size carbon and polyethylene samples were used for calibration purposes.

The neutron sources, source-sample geometries, and neutron-detection systems were identical to those described in ref. [12]. At energies ≤ 4 MeV the neutrons were obtained using the $^7\text{Li}(p,n)^7\text{Be}$ reaction, and at energies > 4 MeV the $\text{D}(d,n)^3\text{He}$ reaction was used [13]. Both reactions emit secondary neutron spectra over a part of the ranges of application. The sources were pulsed at repetition rates of ≤ 2 MHz, with burst durations of ≈ 1 nsec. Burst intensities were enhanced by the use of a harmonic ion-bunching system. Two different cylindrical hydrogenous-scintillator neutron-detection systems were used, having thicknesses of ≈ 2 cm and ≈ 6 cm, respectively. The diameters ranged from ≈ 12.5 cm to ≈ 40 cm depending on flight path. All flight paths were defined by precision collimators inserted through massive shielding. The majority of the measurements were made with scattered-neutron flight paths of ≈ 5 m, with the addition of some higher-resolution measurements using flight paths of ≈ 15 m. The resulting scattered-neutron resolutions were ≈ 0.6 and ≈ 0.2 nsec/m, respectively. At incident energies ≤ 4.0 MeV, the cadmium differential cross sections were determined relative to the total neutron cross section of carbon [14], as described in ref. [15]. The lower-energy techniques are described in more detail in ref. [16]. Above an incident energy of 4 MeV, the cadmium cross sections were determined relative to the $\text{H}(n,n)$ standard cross section [14], as described, for example, in refs. [8 - 12]. All of the experimental results were corrected for sample-attenuation,

multiple-event and angular-resolution effects, and for contributions due to the second neutron group from the ${}^7\text{Li}(p,n){}^7\text{Be}$ source reaction, using Monte-Carlo methods [17].

III. EXPERIMENTAL RESULTS

A. Neutron Elastic Scattering

Detailed measurements of the differential neutron-scattering cross sections of elemental cadmium from a few-hundred keV to 1.5 MeV were made at this laboratory many years ago. They are reported in ref. [18], and will not be further discussed here.

The differential elastic scattering from elemental cadmium was measured from ≈ 1.5 to 3 MeV at ≈ 10 scattering angles distributed between ≈ 20 and 160° and in incident-energy steps of ≈ 100 keV. From 3 to 4 MeV, the elastic-scattering distributions display increasing anisotropy and the number of measurement angles was increased to ≈ 20 at each incident neutron energy, but, as energy-dependent structure was not expected, the incident energy interval was increased to ≈ 200 keV. For incident neutron energies ≤ 4 MeV, the incident-neutron energy spread of ≈ 30 keV and scattered-neutron resolutions were sufficient to define the elastically-scattered component, free of inelastically-scattered contributions. The estimated uncertainties associated with the measured differential values varied from $\leq 5\%$ to larger values at the deep minima of the distributions at the higher energies. These uncertainty estimates include a systematic normalization uncertainty of $\approx 3\%$. The latter estimate is less reliable near 3 MeV where there is considerable structure in the carbon reference cross section, and thus a sensitivity to exact energy scales and calibrations. The 1.5 - 4 MeV elastic-scattering results are summarized in Fig. III-1, and discussed in more detail in the Laboratory report of ref. [16].

From 4.5 to 10 MeV the measurements were made at ≥ 40 scattering angles distributed between $\approx 18^\circ$ and 160° at each incident energy, and at energy intervals of ≈ 500 keV. Two measurement regimes were followed. In the first the scattered-neutron resolution was intentionally selected so as to include inelastically-scattered neutrons due to the excitations < 680 keV (i.e., inclusive of inelastic contributions attributable to the yrast 2^+ levels in the various isotopes). The second regime was applied over the incident-energy interval 5 through 8 MeV. In this energy-range the scattered-neutron resolution was refined so as separate elastically-scattered neutrons from inelastically-scattered components

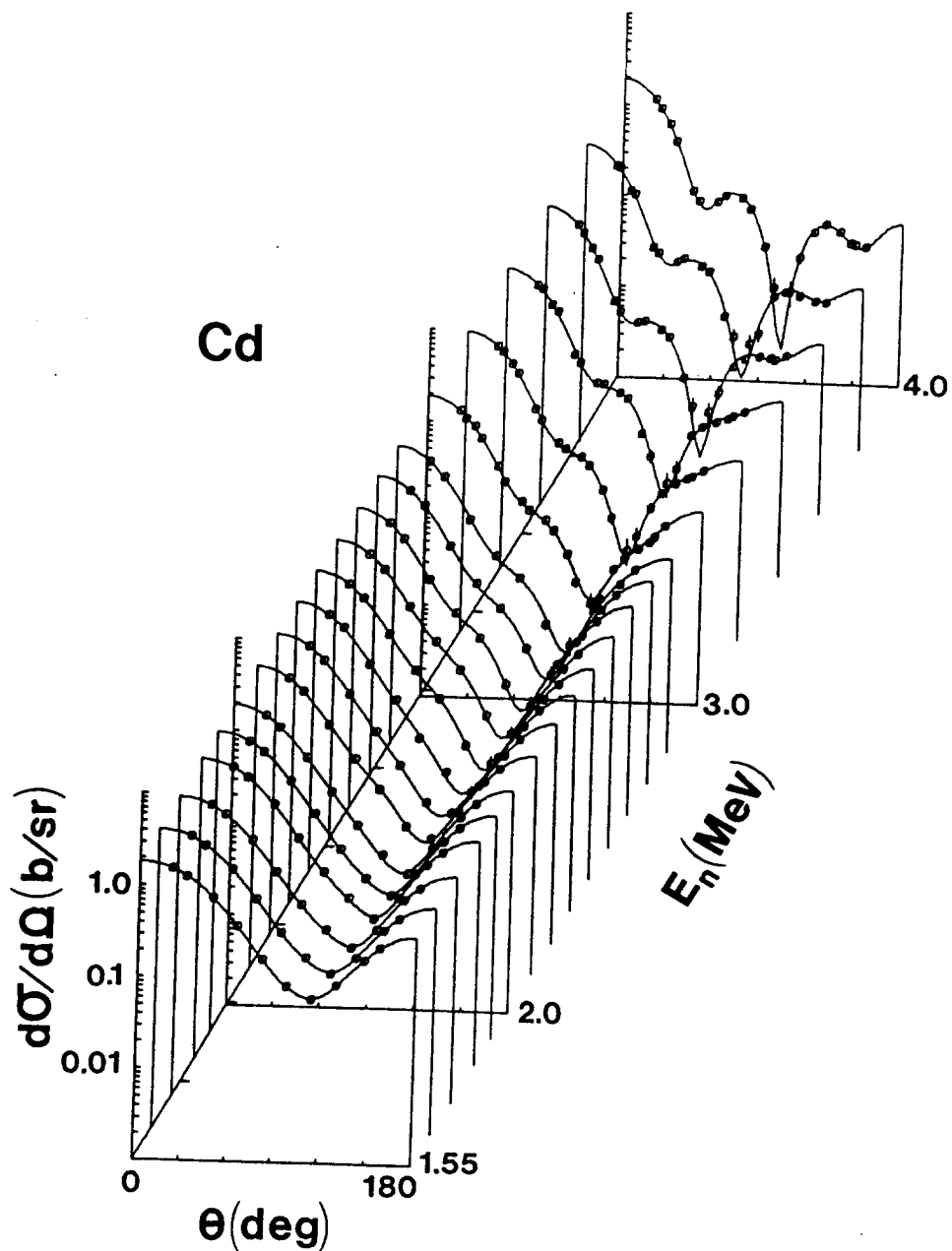


Fig. III-1. Measured differential elastic-scattering cross sections of elemental cadmium in the incident-neutron energy range $\approx 1.5 - 4$ MeV. The experimental values are indicated by symbols, and curves show the results of Legendre-polynomial fits to the measured values. Here, as throughout this paper, angular distributions are given in the laboratory coordinate system.

due to the excitation of levels corresponding to $E_x \approx 600$ ($\pm \approx 300$) keV. The separation was achieved by using care at 5 m flight paths, and also by utilizing the improved resolution available with ≈ 15 m flight paths. Even with this improved resolution, some inelastic contributions due to the excitation of very low-lying levels in the odd isotopes ($\approx 25\%$ abundant) contaminated the observed elastic scattering. These were dealt with in the interpretations as described in Section IV, below. No attempt was made to resolve the low-lying inelastic contributions at 4.5 MeV or above 8 MeV. At the former energy the incident-neutron energy spread from the deuterium-gas target was too large for good resolution, and in the latter energy range the scattered-neutron resolution was insufficient to resolve the low-lying inelastically-scattered contributions. The higher-energy elastic-scattering results are illustrated in Fig. III-2. In this example, the first measurement regime is shown, that including the contributions from the yrast 2^+ levels of the even isotopes and relevant contributions from the odd isotopes, with the elastic component. The figure also shows an ≈ 200 keV average of the lower-energy (≤ 1.5 MeV) results of ref. [18], and an ≈ 250 keV average of the 1.5 - 4 MeV results of the present work, cited above. The estimated uncertainties associated with the measured differential elastic-scattering values above 4 MeV ranged from $\approx 3\%$ to larger values at the minima of the distributions. These uncertainties are inclusive of a 2 - 3% systematic normalization uncertainty, and of an $\approx 0.1^\circ$ uncertainty in the experimental scattering angle. The relative angular scale was determined to better than 0.1° using conventional optical techniques, and the 0° normalization ascertained by observing elastic scattering from a heavy target at both sides of the apparent center line over a range of angles where the cross section is rapidly changing with angle. This zero-angle determination was reproducible. However, it can not be assured that the neutron source position is stable to better than ≈ 1 mm over long measurement periods (many hours to several days), and with the geometries of the measurement system there is a potential for a "flutter" in the scattering angle of $\approx 0.4^\circ$ which could lead to significant cross-section uncertainties at some angles. These were not taken into account as they could not be quantified, or even identified.

Previously reported fast-neutron elastic-scattering cross sections, other than work at this laboratory, appear limited to six distributions [19 - 24]. All of these results are approximately a decade or more old, and some date back nearly forty years. The majority of these results are not consistent with the present work. The discrepancies are qualitatively large, and can not be reasonably explained by experimental considerations such as variations in energy scale and resolution. In view of this situation, comparisons of the present and previous work are not rewarding. There is apparently no experimental information at incident energies above 10 MeV, and this shortfall particularly troubles the physical interpretations of

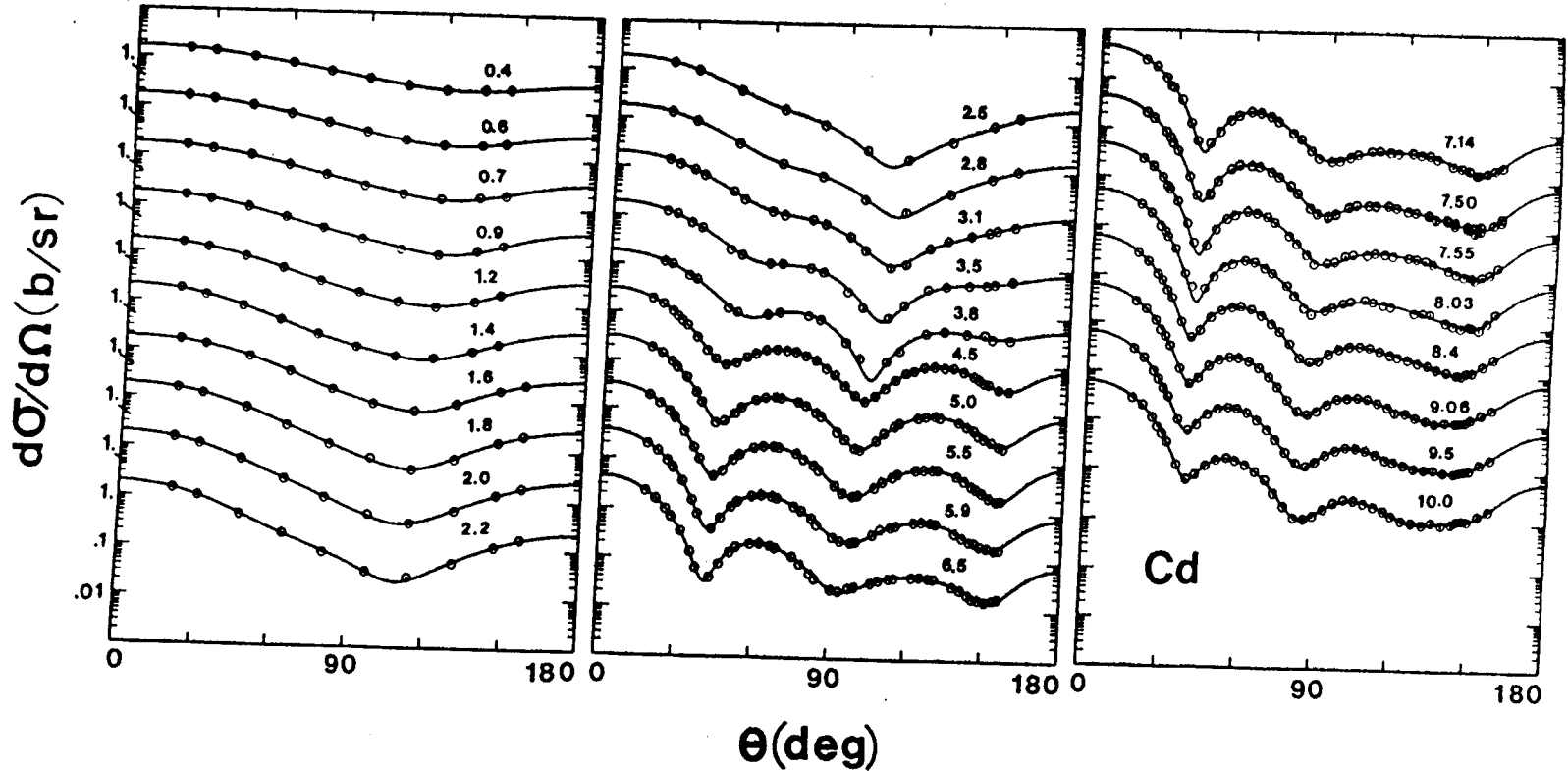


Fig. III-2. Differential elastic scattering cross sections of elemental cadmium. Incident energies (in MeV) are numerically given in each section of the figure. Above 4 MeV the measured values, inclusive of inelastic contributions due to excitations of ≤ 680 keV, are noted by data symbols. Below energies of 4 MeV, averages of the experimental values are noted by symbols as described in the text. Curves are the result of Legendre-polynomial fitting of the measured distributions.

Section IV, below.

B. Neutron Inelastic Scattering

As cited above, there are eight isotopes of elemental cadmium, six of which have abundances of more than a few percent. Two of them are odd isotopes. As a consequence there is a profusion of inelastically-scattered neutron groups, the density of which far exceeds the scattered-neutron energy resolution of the measurement apparatus. This is schematically indicated in Fig. III-3, where the reported excitation energies of the six more abundant isotopes are indicated up to several MeV [3]. This figure also indicates the isotopic abundances for the respective excitations. Of course, the corresponding cross sections will be further modulated by the J^π values and channel competition. The experimental reality is a few prominent neutron "groups", consisting of contributions from several levels, riding on a low continuum background due to contributions from other and unresolved levels, primarily in the odd isotopes. The experimental effect is illustrated by the raw time-of-flight spectrum shown in Fig. III-4. Below ≈ 4 MeV, the measurements were made using the ${}^7\text{Li}(p,n){}^7\text{Be}$ source reaction and flight paths of ≈ 5 m. These measurements lead to the identification of three groups of inelastically-scattered neutrons, corresponding to average excitation energies of 0.589 ± 0.047 , 1.291 ± 0.066 and 1.839 ± 0.057 MeV (where the uncertainties are the RMS deviation of a number of measurements from the mean). These groups are correlated with the known excitation energies as indicated by the diamonds in Fig. III-3. The first two groups approximately correspond to yrast 2^+ levels and the subsequent $0^+-2^+-4^+$ triad of levels in the even isotopes, as outlined in Table III-1, with the addition of some intruding contributions from states in the odd isotopes. Contributions to the 1.839 "group" are more complex, and not clearly related to the underlying isotopic structure. The present measurements extended the results to incident energies of ≈ 8 MeV. Older and lower-energy work from this laboratory [18] partially separated the inelastic contributions from the yrast 2^+ states of the even nuclei.

At incident-neutron energies ≤ 4 MeV, the inelastic-scattering measurements were made concurrently with the above elastic-scattering determinations using the 5 m flight path, and an identical angle-energy mesh. At incident energies in the range 5 - 8 MeV, the majority of the inelastic-scattering measurements were made concurrently with the above elastic-scattering observations, using the 5 m flight paths. With this arrangement the scattered-neutron resolution was marginal at energies of > 7 MeV. Therefore, the short flight path results were supported by 7 and 8 MeV measurements using flight paths of ≈ 15 m at five scattering angles distributed between $\approx 30^\circ$ and 120° . Reasonable experimental resolution was retained at

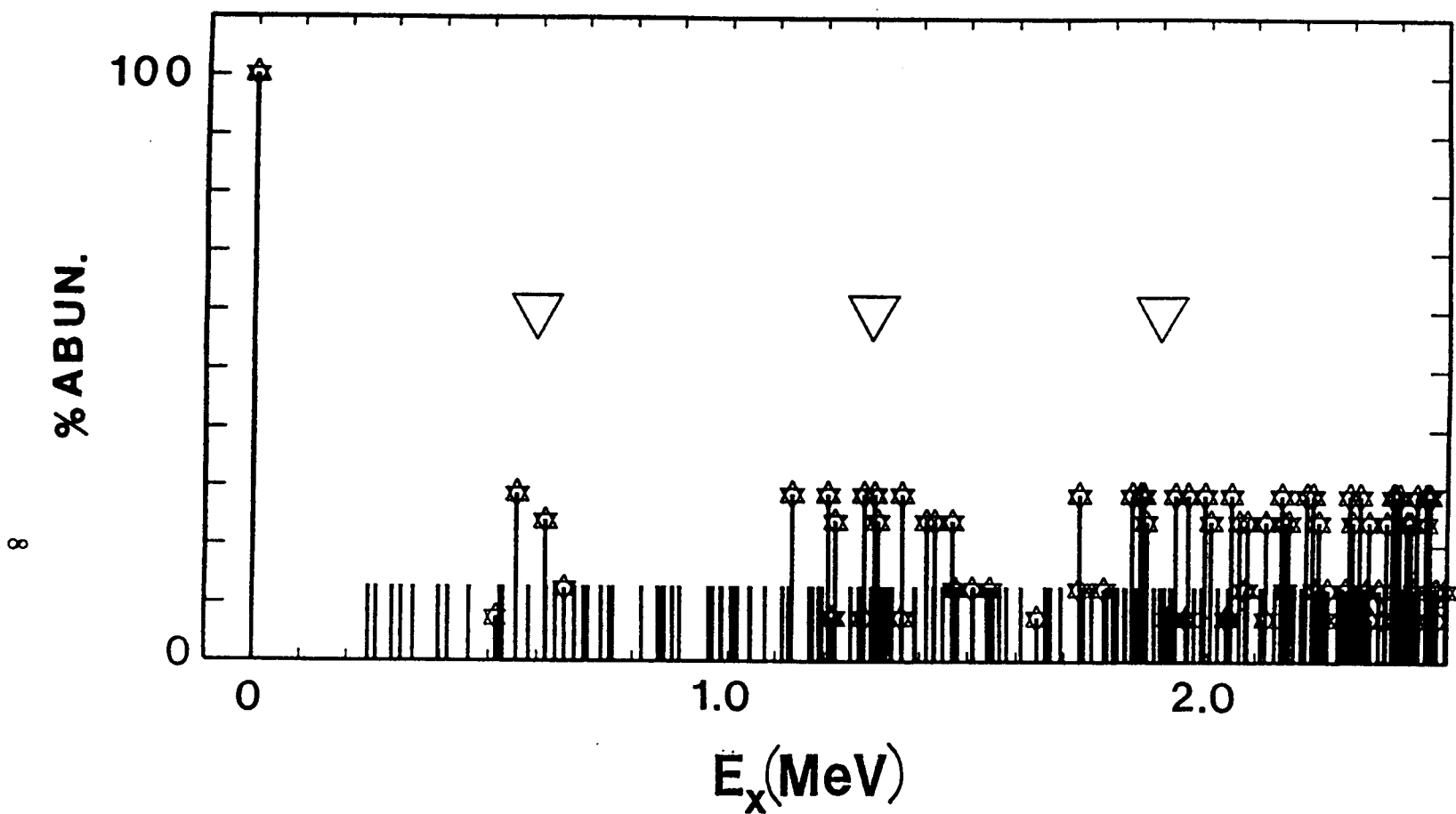


Fig. III-3. Excitation energies in the six prominent isotopes of elemental cadmium [3]. The bar positions indicate level energies, and the bar magnitudes the isotopic abundance (in %) of the respective isotope. "Stars" at bar tips denote even isotopes, and triangles the positions of the observed inelastically-scattered neutron groups.

Table III-1. Low-lying excitations in the five prominent isotopes of elemental cadmium in MeV [3].*

Isotopes:-				
^{110}Cd	^{111}Cd	^{112}Cd	^{113}Cd	^{114}Cd
E_x J^π	E_x J^π	E_x J^π	E_x J^π	E_x J^π
0.000(0^+)	0.000($\frac{1}{2}^+$)	0.000(0^+)	0.000($\frac{1}{2}^+$)	0.000(0^+)
0.658(2^+)	0.245($\frac{5}{2}^+$)	0.618(2^+)	0.264($\frac{11}{2}^+$)	0.558(2^+)
1.473(0^+)	0.342($\frac{3}{2}^+$)	1.224(0^+)	0.298($\frac{3}{2}^+$)	1.135(0^+)
1.476(2^+)	0.396($\frac{11}{2}^-$)	1.312(2^+)	0.316($\frac{5}{2}^+$)	1.210(2^+)
1.542(4^+)	0.417($\frac{7}{2}^+$)	1.415(4^+)	0.458($\frac{7}{2}^+$)	1.284(4^+)
1.731(0^+)	0.620($\frac{5}{2}^+$)	1.433(0^+)	0.522($\frac{7}{2}^-$)	1.306(0^+)
1.783(2^+)	0.680($\frac{9}{2}^-$)	1.469(2^+)	0.530($\frac{7}{2}^+, \frac{9}{2}^+$)	1.364(2^+)
1.809($4^+?$)	0.700($\frac{7}{2}^+, \frac{9}{2}^+$)	1.871(0^+)	0.584($\frac{5}{2}^+$)	1.732(4^+)
2.079(0^+)	0.753($\frac{5}{2}^+$)	2.005(3^-)	0.638($\frac{9}{2}^-$)	1.842(2^+)
2.079(3^-)	0.755($\frac{3}{2}^+$)		0.681($\frac{3}{2}^+$)	1.860(0^+)
2.163(3^+)	0.854($\frac{7}{2}^+$)		0.708($\frac{5}{2}^+$)	1.864(3^+)
2.220(4^+)	0.865($\frac{3}{2}^+$)		0.760($\frac{1}{2}^+$)	
2.287($0^+, 1^+, \underline{2}^+$)			0.820($\frac{7}{2}^+$)	
2.332($\underline{0}^+, 1^+, 2^+$)				
2.356($1^+, \underline{2}^+$)				

* Where alternate J^π values are cited, the underlined values were used in the calculations.

higher energies with these longer flight paths, as illustrated in Fig. III-4. At incident energies < 4 MeV, the angular distributions of the inelastically scattered neutrons were qualitatively symmetric about 90° , and approached isotropy, as would be expected from primarily compound-nucleus reaction mechanisms. Above ≈ 4 MeV, the scattered-neutron angular distributions resulting from the excitation of the first observed "level" increasingly peaked toward forward angles in the manner expected of an appreciable direct-reaction contribution. The significance of these anisotropies is discussed in some detail in Section IV, below. The angle-integrated inelastic scattering cross sections were determined by least-square fitting the measured differential values with Legendre-polynomial expansions. The experimental uncertainties associated with the individual differential inelastic cross sections varied depending on the particular experimental conditions and the neutron group involved. In the better cases, the uncertainties were estimated to be $\approx 10\%$, but increased with decreasing scattering angle and increasing incident energy. These uncertainties were reflected in the angle-integrated values, with an additional factor due to the extrapolation of the fitting procedures to forward angles where no experimental information was available. The resulting angle-integrated inelastic scattering cross sections are summarized in Fig. III-5. The prominent contribution is due to the 598 keV "level", which consists primarily of contributions from the yrast 2^+ states in even isotopes. Similarly, the cross sections for the excitation of the 1.291 MeV "level" are primarily attributed to contributions from the subsequent $0^+-2^+-4^+$ triad of states in the even isotopes. The constituents of the 1.840 MeV "level" are far less certain as there are a variety of states potentially involved, as illustrated in Fig. III-3. Below incident neutron energies of 4 MeV, the accuracies associated with the excitation of the 0.598 MeV "level" are somewhat compromised by elastic scattering due to the second neutron group from the ${}^7\text{Li}(p,n){}^7\text{Be}$ source reaction. Corrections for this perturbation were made, but they did increase the uncertainty.

There appears to be no comparable experimental inelastic-scattering results reported in the literature other than the early low-energy work from this laboratory, described in ref. [18]. The latter extends up to only ≈ 1.5 MeV, but the results are reasonably consistent with the present values, as shown in Fig. III-5.

IV. PHYSICAL INTERPRETATION

The following interpretations had several objectives:- i) Provide a conventional spherical-optical-model (SOM) potential for the parameterization of the fast-neutron interaction with cadmium, suitable for subsequently addressing basic and applied issues. ii) Consider possible implications of the dispersive-optical-model (DOM)

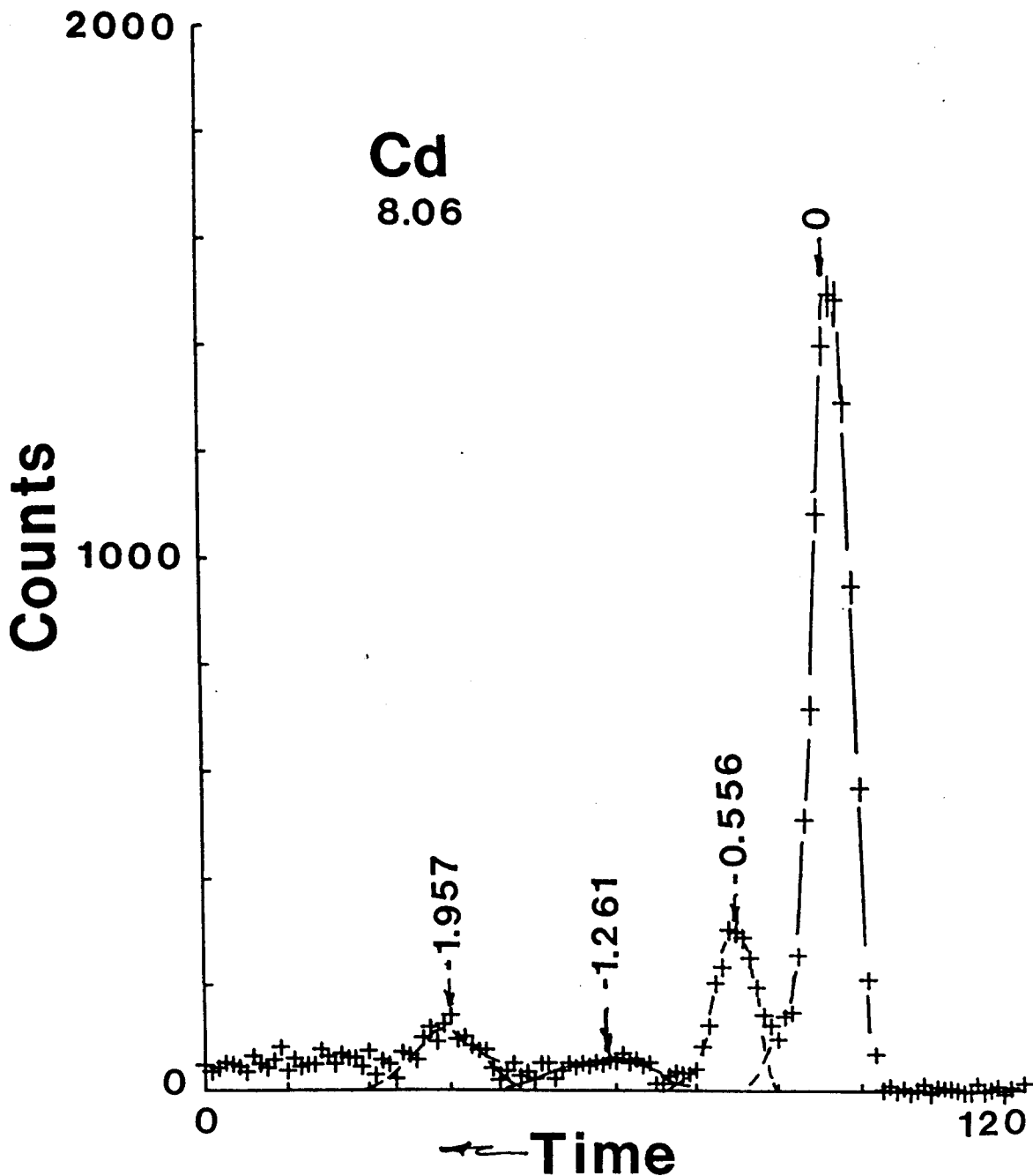


Fig. III-4. Illustrative higher-energy time-of-flight spectrum obtained by scattering 8.06 MeV neutrons from elemental cadmium, over a flight path of ≈ 15 m, through a scattering angle of 80° . Numerical values indicate excitation energies (in MeV) as determined from this particular measurement. The horizontal axis is an arbitrary instrument time scale with time increasing from right to left.

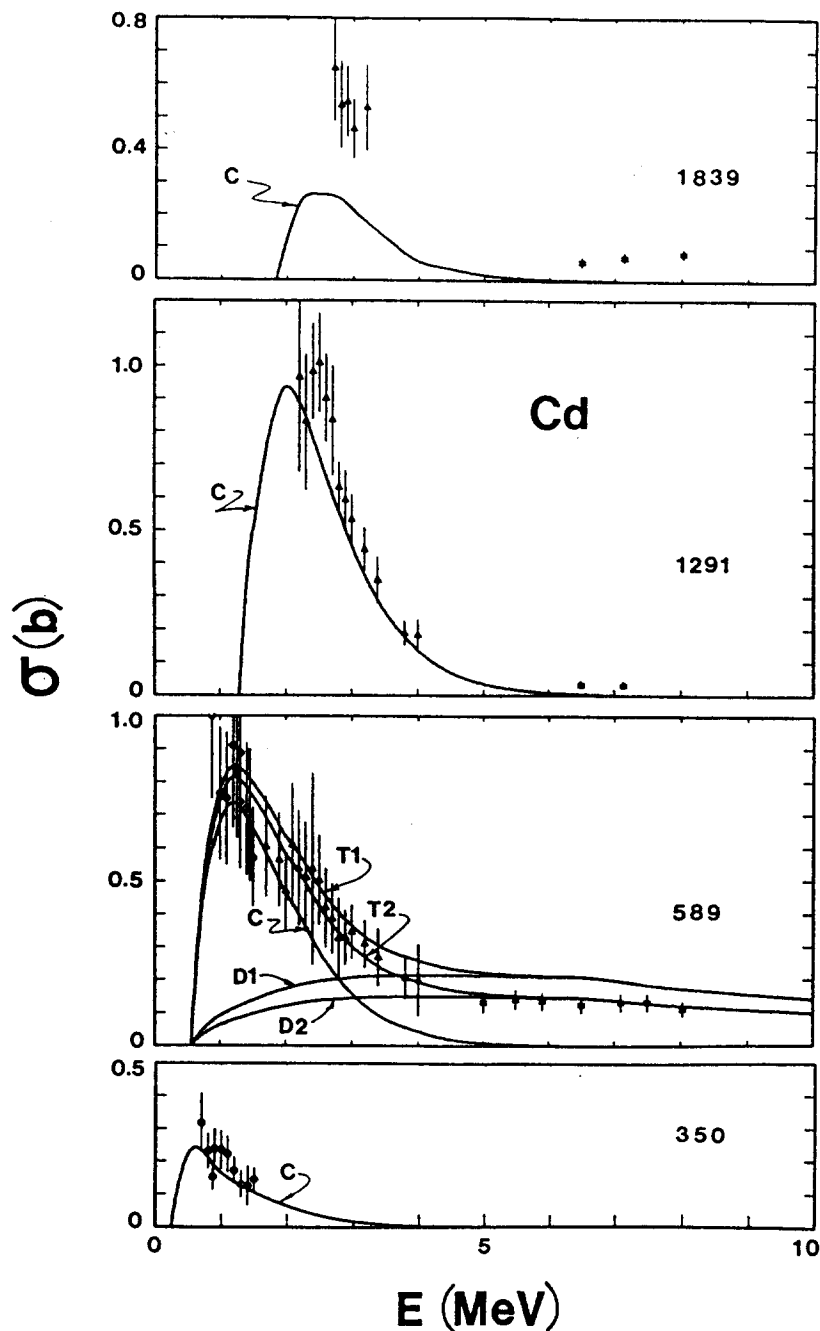


Fig. III-5. Measured inelastic scattering cross sections of elemental cadmium. Experimental values of the present work are indicated by ∇ and $*$ symbols, and those of ref. [18] by \circ . Observed excitation energies (in keV) are numerically given in each portion of the figure. The curves indicate the results of calculations as follows; "C" = compound-nucleus components, "D1" = direct excitations calculated using the one-phonon model, "D2" = direct excitations calculated with the one- and two-phonon model, "T1" = total excitations (inclusive of the compound-nucleus contribution) using the one-phonon model, and "T2" = total excitations using the one- and two-phonon model.

potential. iii) Examine collective effects assuming a vibrational coupling in the context of the coupled-channels-model (CCM), and the capability to describe the direct inelastic-scattering processes. The use of the present experimental results to assess the correlation of neutron-transition matrix elements with electro-magnetic properties is discussed elsewhere [4]. An inherent problem throughout these interpretations (and in the measurements) is the multi-isotopic nature of elemental cadmium, cited above. The abundances of ^{106}Cd and ^{108}Cd are very small, and thus they are ignored in the present interpretations. ^{116}Cd has nuclear structure similar to that of ^{114}Cd and is less than 7.5% abundant, thus it too was ignored. The remaining five isotopes were dealt with as described in the following sections.

A. The Spherical Optical Model (SOM)

This portion of the interpretation utilized a special version of the SOM calculation code ABAREX [25] which is capable of calculating isotopic cross sections, including explicit treatment of the individual isotopic excited structures, and combining them to obtain elemental cross sections comparable with observations. The respective excitation energies and J^π values were taken from ref. [3], as given in Table III-1. These include fifteen levels for ^{110}Cd , twelve for ^{111}Cd , nine for ^{112}Cd , thirteen for ^{113}Cd and eleven for ^{114}Cd . The relative isotopic abundances of these five isotopes were normalized to a total of 100%. Compound-nucleus processes were calculated using the Hauser-Feshbach theory [26], with the width fluctuation corrections of Moldauer [27]. At energies above the well known discrete excitations, a continuum of levels in each isotope was represented using the statistical formalism of Gilbert and Cameron [28]. Throughout this work, it was assumed that the potential consisted of a Saxon-Woods real form, a Saxon-Woods-derivative imaginary term, and a Thomas spin-orbit component [29]. All of the potential parameters were deduced by chi-square fitting the measured elastic-scattering data base. The results of the fitting were then subjectively compared with the measured neutron total cross sections, observed inelastic-scattering cross sections, and with reported strength functions deduced from resonance measurements.

The elastic-scattering data base was constructed from the measured values of the present work, extended to lower energies with previously-reported work at this laboratory [18]. At the low energies there is some total-cross-section evidence of residual fluctuating structure [30]. Therefore, the low-energy elastic-scattering distributions of ref. [18] were averaged over energy increments of ≈ 0.2 MeV. From 1.5 to 4 MeV, the present work provides twenty elastic-scattering distributions. This is a large body of

experimental information, therefore it was averaged over energy increments of ≈ 250 keV in order to reduce the amount of data handled in the numerical calculations and, at the same time, to smooth any physical or experimental fluctuations that may be present. Above 4 MeV, the data base explicitly consisted of the measured values of the present work. As outlined above, for energies ≤ 4 MeV, the data base consisted of essentially true elastic-scattering distributions. At higher energies the data was handled in two ways. On one hand, the high-resolution measured values were used. These consisted primarily of the prominent elastic-scattering contribution, with the addition of a relatively small perturbation from inelastic scattering due to the excitation of the first several low-lying levels of the odd isotopes. Alternatively, the lesser-resolution results were used, which are inclusive of inelastic contributions from the assumed one-phonon levels in the even isotopes, and the first six excitations of the odd isotopes. The numerical fitting procedures were arranged to correspond to these alternate experimental resolutions using the capability of ABAREX to fit cross sections due to a composite of levels, as well as single levels. A large share of this data base is illustrated in Fig. III-2.

There seems to be no information on the polarization of neutrons elastically-scattered from cadmium. Therefore, throughout these interpretations the "global" real spin-orbit potential of ref. [31] was assumed (see Table IV-1). Experience indicates [32] that the real-potential geometry tends to be less sensitive to the details of nuclear structure than that of the imaginary potential, therefore it was determined first. From six-parameter fitting of the elastic-scattering data (real and imaginary strengths, radii, and diffusenesses) the real-potential diffuseness, a_v , was first fixed. It was found to be essentially energy independent. Next, from five-parameter fits (a_v held fixed) the real-potential radius, r_v , was determined. It too was essentially energy independent, though there remain some uncertainties as there is a well known correlation between real-potential strengths and radii [29,33]. In a similar manner the geometry of the imaginary potential was determined, using four parameter fits to determine the imaginary-potential radius and three parameter fits to fix the imaginary-potential diffuseness (again, there are uncertainties in the latter parameter due to the strong correlation between the imaginary strength and diffuseness [29,33]). Finally, two parameter fits (with the geometries fixed as discussed above) were used to determine the real- and imaginary-potential strengths. The results of the two-parameter fitting are compared with the data base in Fig. IV-1. The description of the measured data is very good except at the first minima of the distributions near ≈ 6 MeV. In this mass-energy-angle region SOM calculations lead to very deep minima. As shown in Section IV-C, these minima are, to a considerable extent, artifacts which vanish when vibrational coupling is taken into account. Such vibrational effects are not consistent with the assumptions underlying the SOM, and thus one should expect some shortcomings in the descriptions of the measured values. An additional factor in these minima is the energy spread of the neutron

source. This is relatively very small at 10 MeV (≈ 100 keV), but at 4.5 MeV the deuterium gas cell used as a neutron source becomes quite "thick" (e.g., 300 \rightarrow 600 keV), depending upon the gas pressure used in the particular measurement. When the calculated results are averaged over a comparable energy spread the cross-section magnitudes in the shape first minima are increased by factors of 2 \rightarrow 5.

The SOM potential parameters, resulting from the above fitting procedures, are given in Table IV-1. The parameterizations of the SOM potential strengths are illustrated in Fig. IV-2, together with the results of the fitting procedures. The physical implications of the SOM are discussed in Section V. However, briefly the real-potential strength, J_v , decreases with energy in a manner qualitatively consistent with Hartree-Fock predictions (herein all potential strengths are cited in terms of volume-integrals-per-nucleon, J_i). The imaginary-potential radius, r_w , decreases with energy, and the corresponding diffuseness, a_w , increases with energy. Concurrently, the imaginary-potential strength, J_w , decreases with energy. The J_w character is not typical of the SOM of a spherical nucleus.

The SOM parameterization gives a reasonable description of the neutron total cross section over a wide energy range, as illustrated in Fig. IV-3. In making this comparison, it was assumed that the imaginary-potential parameters were energy independent above 10 MeV, taking the 10 MeV values of Table IV-2. The calculated neutron total cross section agrees with energy averages of the measured values given in the literature [30,34 \rightarrow 50] to within $< 5\%$ from 100 keV to more than 25 MeV. The SOM parameters also provide a reasonable description of the measured inelastic-scattering cross sections in regions where the compound-inelastic-scattering component is the dominant contribution, as illustrated in Fig. III-5. At the higher energies the SOM can not describe the significant direct inelastic-scattering cross sections. Finally, the strength functions calculated with the SOM are compared with those deduced from resonance measurements [51] in Table IV-2. In making these strength-function comparisons it was assumed the the real and imaginary isovector strengths were 24 and 12 MeV, respectively. The comparisons are not sensitive to these choices. The agreement is reasonably good, given the scatter of the values deduced from experiment.

B. The Dispersive Optical Model (DOM)

It is well known [52] that the dispersion relationship correlates real, V , and imaginary, W , portions of the optical potential through the expression

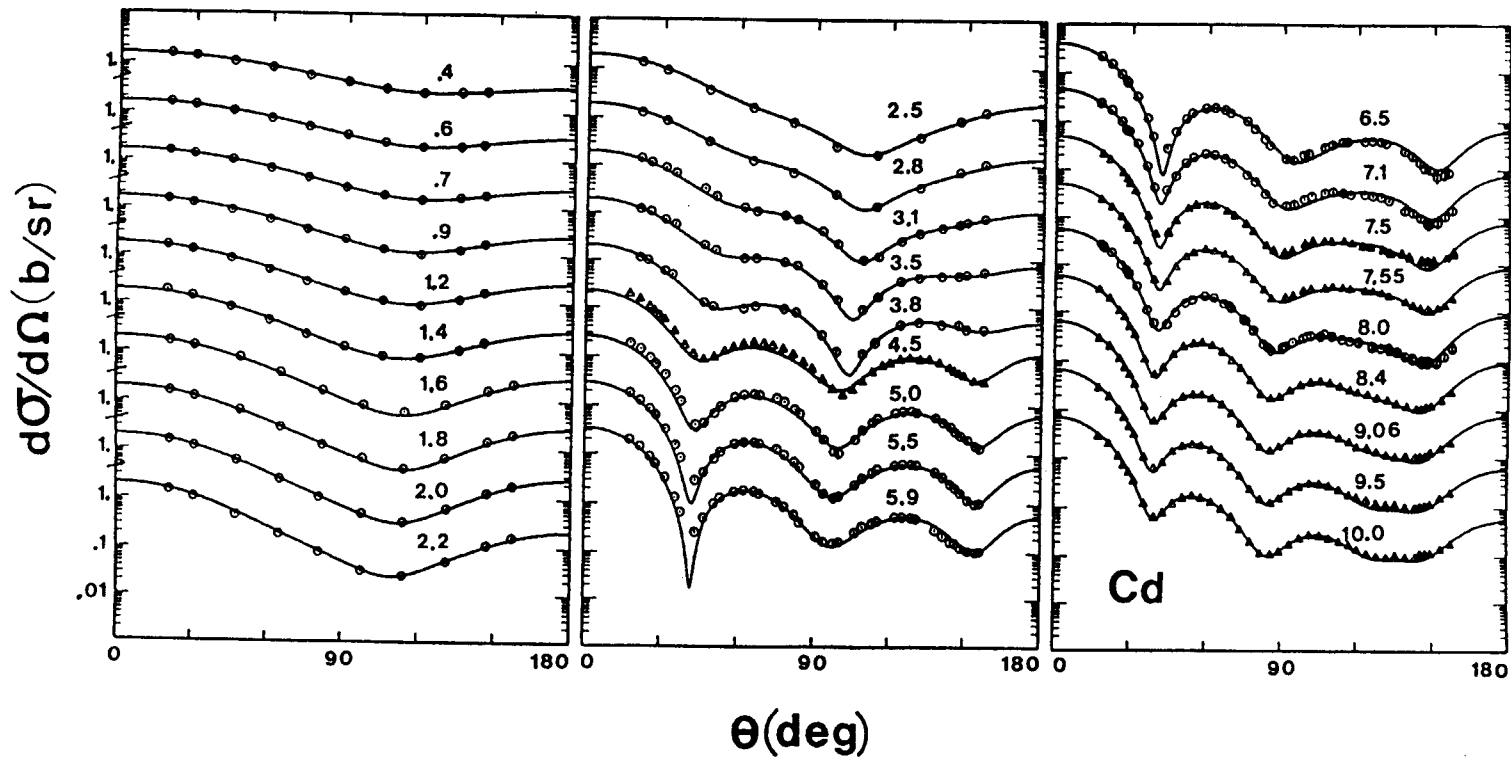


Fig. IV-1. Comparison of measured and calculated differential elastic-scattering cross sections of cadmium. The experimental values are denoted by "o" (elastic scattering) and "Δ" (elastic- plus inelastic-scattering due to the excitation of the low-lying levels, as discussed in the text). Curves indicate the comparable results calculated from the two parameter SOM fitting described in the text.

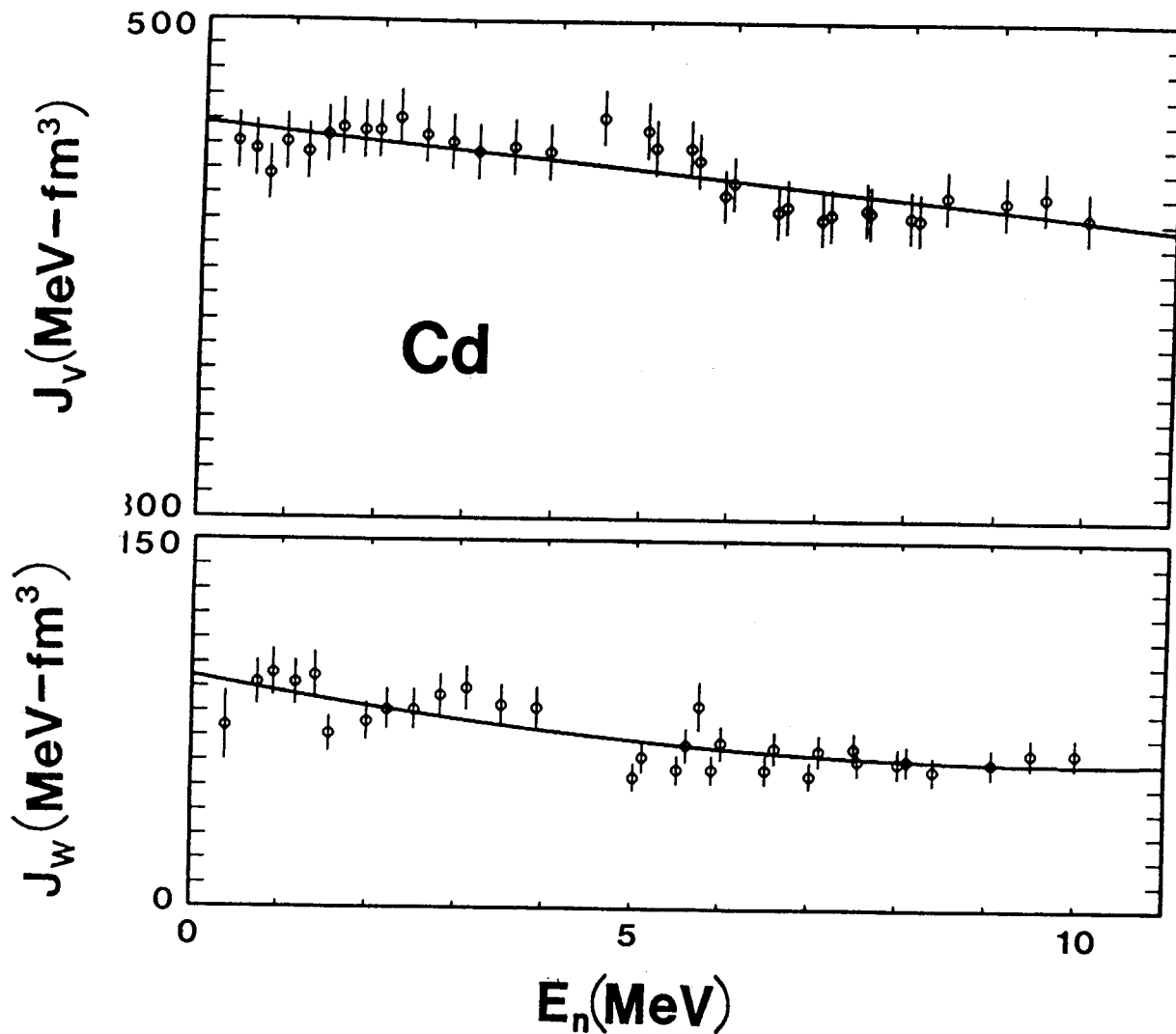


Fig. IV-2. Real, J_v , and imaginary, J_w , SOM potential strengths expressed as volume-integrals-per-nucleon. Symbols indicate the results of the fitting procedures described in the text, and curves the parameterizations of Table IV-1.

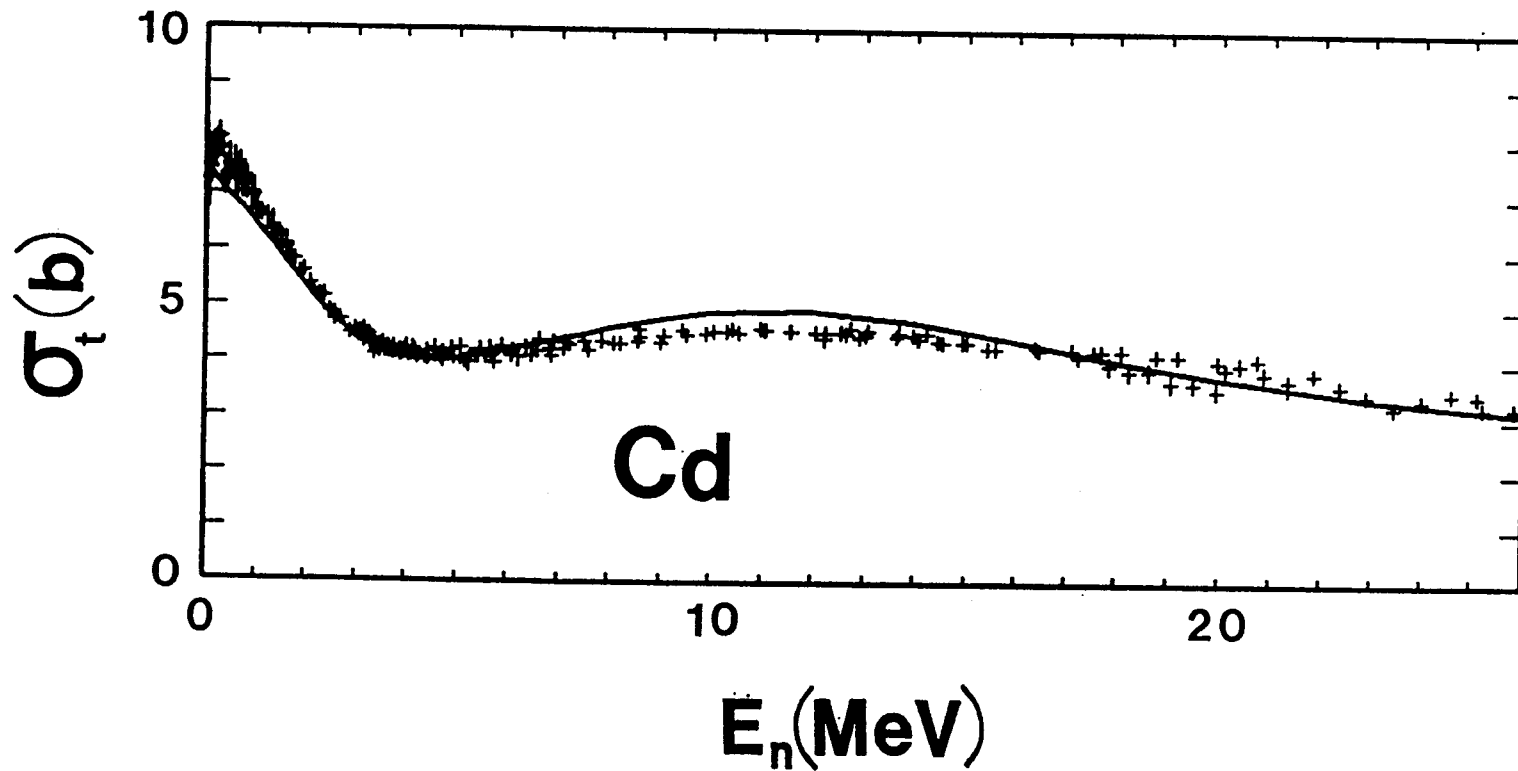


Fig. IV-3. Comparison of energy averages of measured neutron total cross sections of cadmium [30,34 → 50] (symbols) with the results of calculations using the S₀M parameters of Table IV-1 (curve).

Table IV-1. Parameters of the SOM potential. All geometries are expressed in fermis, energies in MeV, and real- and imaginary-potential strengths in volume-integrals-per-nucleon, J (in units of MeV-fm³). The parameterization is rigorously valid only up to 10 MeV, as discussed in the text.*

Real Potential (V)

$$J_v = 458.6 - 3.759 \cdot E$$

$$r_v = 1.3023$$

$$a_v = 0.6272$$

Imaginary Potential (W)

$$J_w = 94.6 - 6.801 \cdot E + 0.331 \cdot E^2$$

$$r_w = 1.3790 - 0.01278 \cdot E$$

$$a_w = 0.3485 + 0.0178 \cdot E$$

Spin-Orbit Potential (S0)

$$V_{so} = 6.0588 - 0.015 \cdot E$$

$$r_{so} = 1.103$$

$$a_{so} = 0.560$$

* Numerical parameters are given to precision permitting quantitative reproduction of the calculated results.

Table IV-2. Comparisons of SOM calculated strength functions for the prominent cadmium isotopes with those deduced from experimental measurements (in parenthesis) [51].

Isotope	S_0^*	S_1^*
^{110}Cd	0.723 (0.44±0.11)	3.58 (3.0±1.0)
^{111}Cd	0.725 (0.8±0.2)	3.56 (3.0±1.5)
^{112}Cd	0.727 (0.5±0.1)	3.54 (4.4±1.0)
^{113}Cd	0.730 (0.31±0.07)	3.52 (2.2±0.8)
^{114}Cd	0.732 (0.64±0.16)	3.50 (3.5±1.0)

* In units of 10^{-4} .

$$V(r,E) = V_{\text{HF}}(r,E) + \frac{P}{\pi} \int_{-\infty}^{+\infty} \frac{V(r,E')dE'}{(E-E')}, \quad (\text{IV-1})$$

where P denotes the principal value of the integral and V_{HF} the Hartree-Fock potential. This relationship influences the geometries and strengths of the SOM, and leads to the "Fermi Surface Anomaly" at lower energies [53]. These effects were assessed by re-interpreting the experimental data base taking into account Eq. IV-1.

It is convenient to carry out the DOM interpretation in terms of the volume-integrals-per-nucleon, J_i . In that form, Eq. IV-1 becomes

$$J_v = J_{\text{HF}} + \frac{P}{\pi} \int_{-\infty}^{+\infty} \frac{J_w(E')dE'}{(E-E')}, \quad (\text{IV-2})$$

where the integral can be broken into surface, ΔJ_s , and volume, ΔJ_{v0} , components. Then

$$\begin{aligned} \Delta J_s(E) &= \frac{P}{\pi} \int_{-\infty}^{+\infty} \frac{J_s(E')dE'}{(E-E')} \\ \Delta J_{v0}(E) &= \frac{P}{\pi} \int_{-\infty}^{+\infty} \frac{J_{v0}(E')dE'}{(E-E')}, \end{aligned} \quad (\text{IV-3})$$

and

$$J_v(E) = J_{\text{eff}}(E) + \Delta J_s(E), \quad (\text{IV-4})$$

where $J_{\text{eff}}(E) = J_{\text{HF}}(E) + \Delta J_{v0}(E)$, assumed to have the same Saxon-Woods geometries. The present SOM interpretation (Section IV-A, above) gives no support for a volume absorption up to at least 10 MeV. Furthermore, ΔJ_{v0} and J_{HF} are approximately linear functions of energy from at least from -20 to +20 MeV, thus the J_{HF} and ΔJ_{v0} components of J_{eff} are not experimentally separable. It is useful to define the ratio

$$\lambda(E) = \Delta J_s(E)/J_s(E), \quad (\text{IV-5})$$

where $\lambda(E)$ is the quantity by which the surface-imaginary potential, J_s , is multiplied to give the surface-peaked component of the real potential, ΔJ_s .

The SOM of Section IV-A, above, was used to evaluate $\lambda(E)$ of Eq. IV-5. Simple approximations, that have been widely employed at this laboratory and elsewhere [10,32], were used. Very briefly, they are:-

J_s was assumed symmetric about the Fermi Energy, E_F . E_F was taken to be -7.895 MeV, the weighted average of the values for the eight isotopes of the element. For energies $2 \cdot E_F < E < 0$, J_s was assumed to have the form $J_s = (J_0/E_F^2)(E-E_F)^2$, where J_0 is the value of J_s as $E \rightarrow 0$. For $0 < E < 15$ MeV, J_s was assumed to have the form given in Table IV-1. For $E > 15$ MeV, J_s was assumed to linearly decrease with energy to a zero value at 60 MeV. The choice of 15 MeV as the break point in J_s is rather arbitrary as there is no experimental information to determine the behavior above ≈ 10 MeV. However, it is reasonable to expect that volume absorption will start to become a factor at ≈ 15 MeV, with a consequent decrease in J_s with energy. The behavior of ΔJ_s calculated with these assumptions is shown in Fig. IV-4, together with the corresponding $\lambda(E)$. The overall effect is to add a significant surface term to the Saxon-Woods Hartree-Fock real potential over the whole energy range of the present interpretations (i.e., for $E = 0 \rightarrow 10$ MeV).

The entire fitting procedure of Section IV-A was repeated including the surface component of the real potential determined from $\lambda(E)$, calculated with the above assumptions and shown in Fig. IV-4. The resulting DOM parameters (see Table IV-3) gave a description of the elastic-scattering data base of essentially the same character as that obtained with the SOM, as indicated by a comparison of Figs. IV-1 and -5. Differences between the results obtained with the two models are a matter of minor detail. The neutron total cross sections calculated with the DOM are perhaps somewhat more suitable than those obtained with the SOM at the higher energies and somewhat less suitable at the very low energies, as illustrated by comparison of Figs. IV-3 and -6. The behavior of $\lambda(E)$ at very low energies is probably little more than qualitative, and this may impact upon the calculation of low-energy cross sections. However, the strength functions calculated with the DOM, given in Table IV-4, are very similar to those obtained with the SOM (Table IV-2).

The DOM real-potential radius is somewhat smaller than that of the SOM, as is expected since the ΔJ_s surface component of the potential has been explicitly treated. Similarly, the real diffuseness of the DOM is somewhat larger than that of the SOM as the contribution of the narrow ΔJ_s surface component has been removed. The SOM and DOM imaginary radii are very similar, and the minor differences are probably of no significance. Likewise, the imaginary-potential diffusenesses of the two models are essentially identical. The fact that a quadratic rather than linear representation emerged for the DOM is probably a statistical artifact, and the quadratic coefficient in the DOM representation is very small. The strengths of the DOM real and imaginary potentials, given in Table

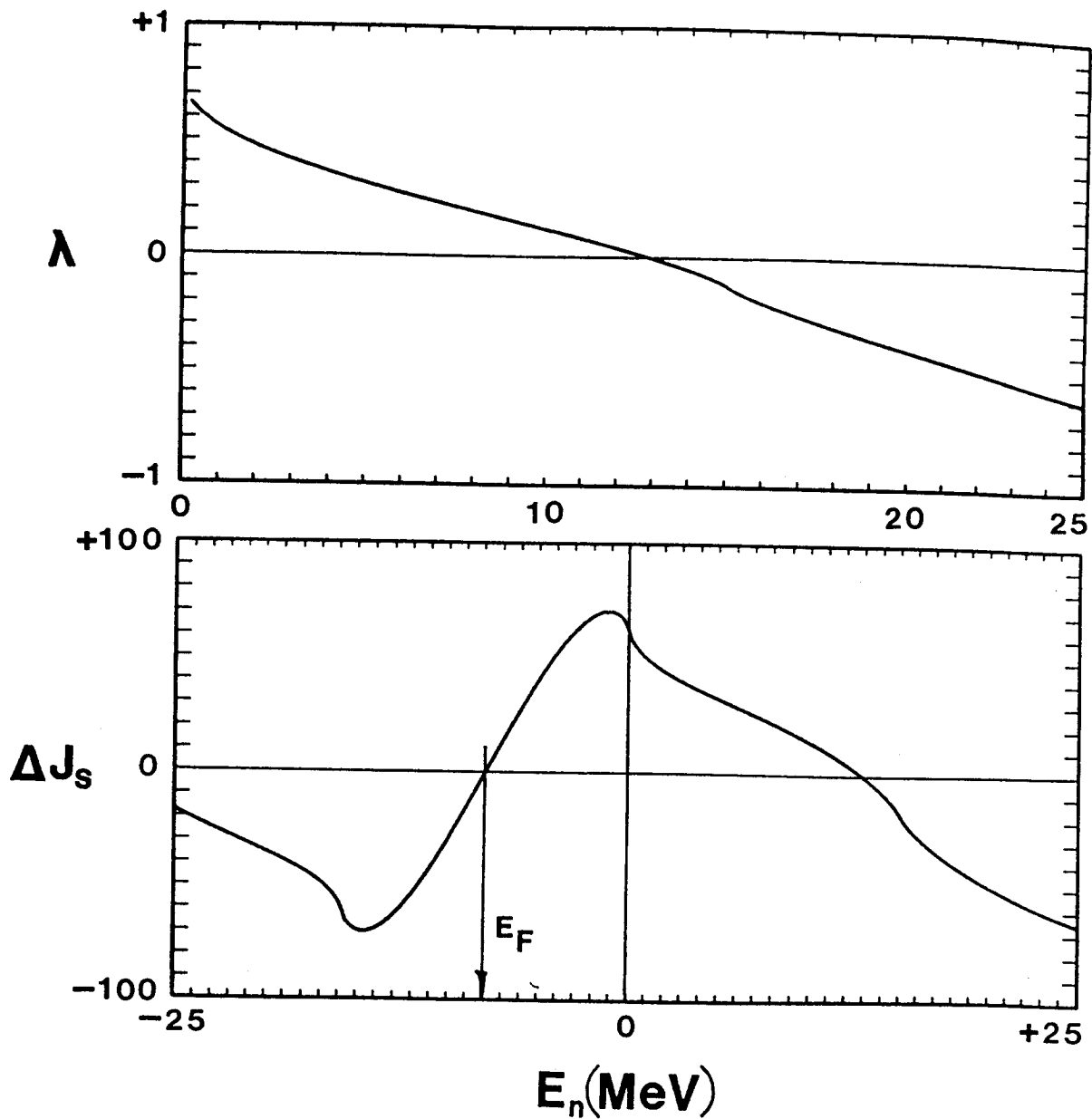


Fig. IV-4. The energy dependence of $\lambda(E)$ of Eq. IV-5 (top), and of $\Delta J_s(E)$ of Eq. IV-3 (bottom). ΔJ_s is given in units of $\text{MeV}\cdot\text{fm}^3$.

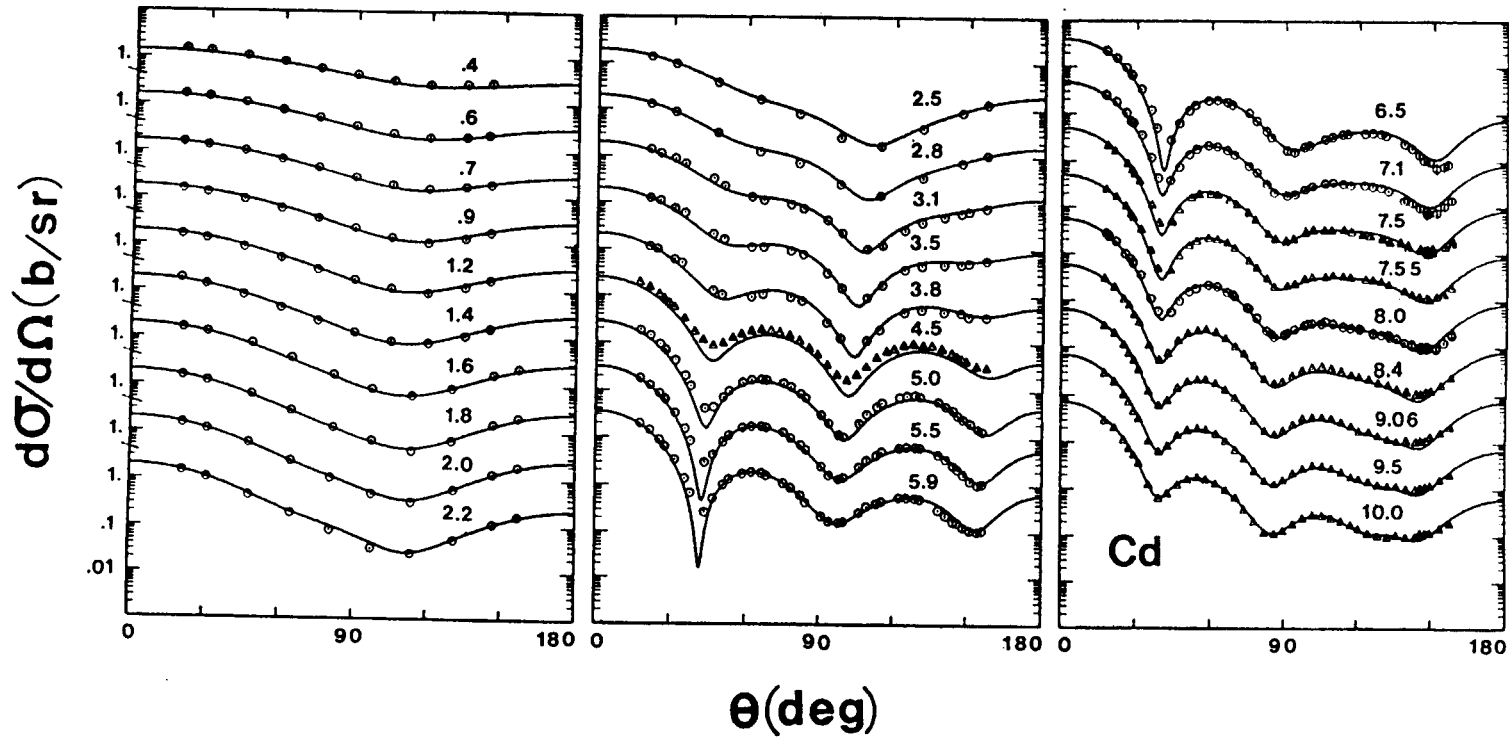


Fig. IV-5. Comparison of measured (symbols) and calculated (curves) differential elastic-scattering cross sections of cadmium. The calculations were made using the DOM, and the notation is identical to that of Fig. IV-1.

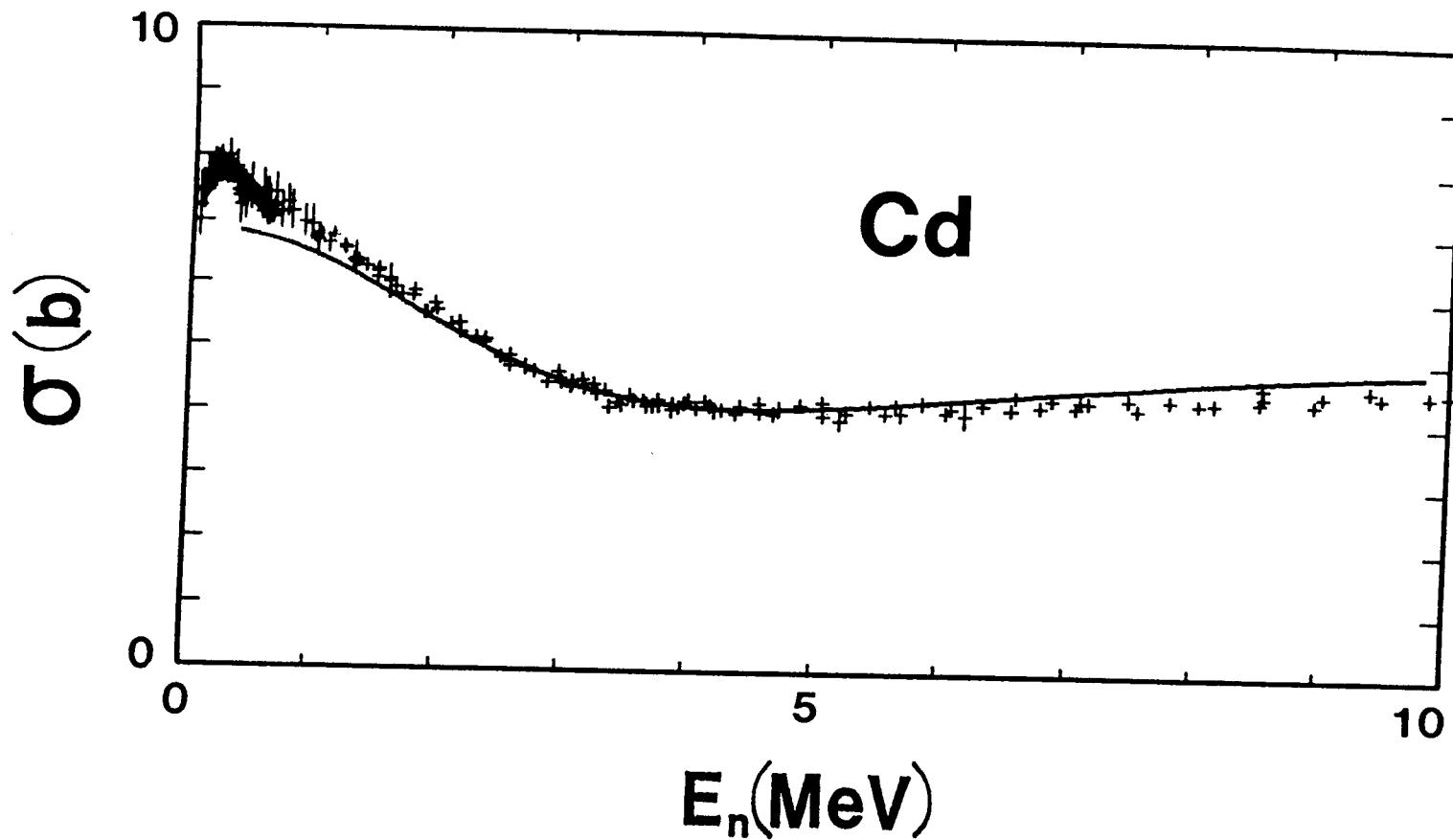


Fig. IV-6. Comparison of measured (symbols) and calculated (curve) neutron total cross sections of cadmium. The calculations were made using the DOM of the text.

Table IV-3. Parameters of the DOM potential. The notation is identical to that of Table IV-2. The parameterization is rigorously valid only up to 10 MeV, as discussed in the text.

Real Potential (V)

$$J_v = 426.0 - 1.528 \cdot E$$

$$r_v = 1.2765$$

$$a_v = 0.6692$$

Imaginary Potential (W)

$$J_w = 105.1 - 9.5418 \cdot E + 0.52221 \cdot E^2$$

$$r_w = 1.384 - 0.01366 \cdot E$$

$$a_w = 0.3385 + 0.02537 \cdot E - 0.000750 \cdot E^2$$

Spin-Orbit Potential (S0)

Identical to that given in Table IV-1.

Table IV-4. Comparisons of DOM calculated strength functions for the prominent cadmium isotopes with those deduced from experimental measurements (in parenthesis) [51].

Isotope	S_0^*	S_1^*
^{110}Cd	0.733 (0.44±0.11)	3.26 (3.0±1.0)
^{111}Cd	0.745 (0.8±0.2)	3.15 (3.0±1.5)
^{112}Cd	0.750 (0.5±0.1)	3.04 (4.4±1.0)
^{113}Cd	0.762 (0.31±0.07)	2.93 (2.2±0.8)
^{114}Cd	0.770 (0.64±0.16)	2.83 (3.5±1.0)

* In units of 10^{-4} .

IV-3, are illustrated in Fig. IV-7. The real-potential strength of the DOM (actually, J_{eff} of Eq. IV-4) is less than that of the SOM (Table IV-1), with a smaller energy-dependent slope. This is consistent with the magnitude of ΔJ_s and the energy dependence of $\lambda(E)$ shown in Fig. IV-4. The imaginary-potential strength of the DOM is qualitatively similar to that of the SOM. In both cases the imaginary strength decreases with energy, contrary to what one would expect. The physical implications of some of these properties is further discussed in Section V.

C. The Coupled-Channel Vibrational Model (CCM)

The isotopes of elemental cadmium display collective features [3,54]. For example, there are two-phonon states in the even isotopes at about twice the energies of the one-phonon levels. On the other hand, the yrast 2^+ levels have non-vanishing quadrupole moments indicating the nuclei are not simple vibrators. Collective aspects of the neutron interaction with these isotopes are also evident in the present experiments; e.g. in the inelastic-scattering processes. In the present model derivation it was assumed that the cadmium isotopes are simple one-phonon vibrators. The respective β_2 values derived from electro-magnetic studies are given in the compilation of ref. [54], leading to the weighted-average value for the even isotopes of $\beta = 0.1867$. The corresponding value for the neutron processes should be somewhat larger [55]. However, for the present interpretation a mean value of $\beta_2 = 0.175$ was assumed, as deduced from the theoretical considerations of ref. [4]. This value is somewhat smaller than that implied by ref. [54] as it was derived from the more-recent Nuclear Data Sheets of ref. [3], and is inclusive of the odd-isotope contributions.

The parameters of the CCM were determined in a manner analogous to that pursued in the SOM and DOM interpretations, with the same sequence of chi-square fitting the measured elastic-scattering distributions. However, because of the tedious nature of the calculations, it was assumed that the neutron interaction was with a single "effective" even nucleus with a mass $A = 112.5$, and having the yrast 2^+ level at 586 keV [4]. Higher-energy excitations, and the continuum, were taken to be those of ^{112}Cd . The compound-nucleus contribution was explicitly treated in the fitting up to incident energies of ≈ 2.3 MeV. At higher incident energies corrections were made for compound-nucleus contributions using the above SOM. They were small, and became negligible above ≈ 6.5 MeV. The CCM calculations were carried out with the computing program ANLECIS [56]. The resulting CCM parameters are summarized in Table IV-5. These parameters provide a very good description of the elastic-scattering data base from which they were derived, as illustrated in Fig. IV-8.

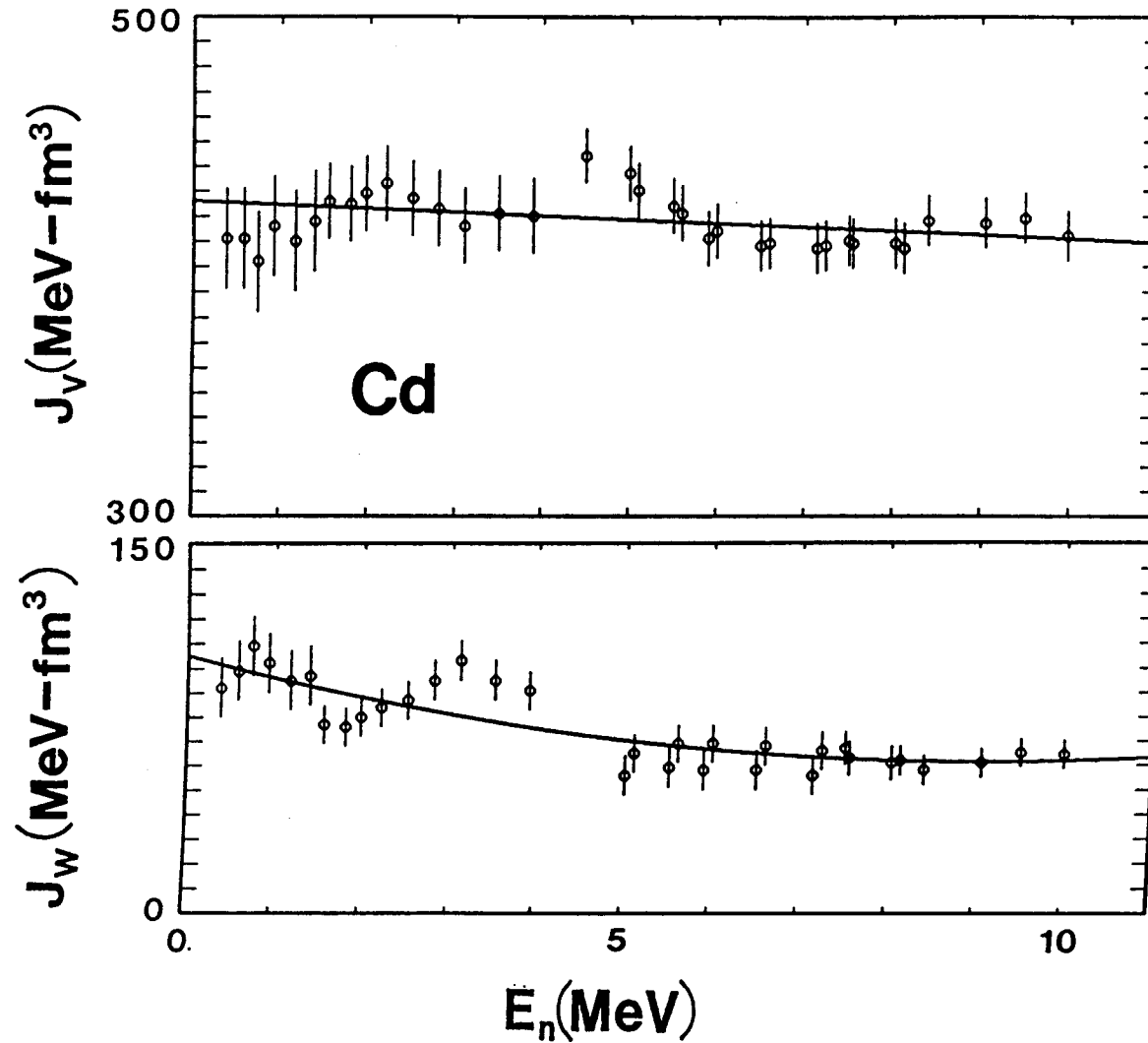


Fig. IV-7. Real, J_v , and imaginary, J_w , DOM potential strengths expressed as volume-integrals-per-nucleon. Symbols indicated the results of the fitting procedures described in the text, and curves the parameterizations of Table IV-3.

In particular, the sharp minima of the elastic distributions in the energy range 5 - 6 MeV, obtained with the spherical models (Figs. IV-1 and -5), have vanished, resulting in a greatly improved description of the measured values. The total cross sections calculated with the CCM are essentially identical to those obtained using the SOM (Fig. IV-3) above ≈ 1 MeV. At lower energies they are a few percent smaller than those obtained with the SOM. This is probably due to a J_v value as $E \rightarrow 0$ that is slightly too large, and the three lowest-energy values, shown in Fig. IV-9, are below the general linear trend indicated by the body of the J_v data. This may represent a local fluctuation or an experimental artifact, and the lowest energy values are from very old data [18]. The $l = 0$ strength function calculated with the CCM is ≈ 0.42 , or about 57% that obtained with the SOM. However, the value remains in the mid-range of those deduced from resonance measurements, as shown in Tables IV- 3 and -5. With the scatter in the values deduced from resonance measurements, comparisons of measured and calculated strength functions remain less than definitive.

The CCM parameters of Table IV-5 differ from those of the SOM as indicated by the numerical simulations of ref. [57,58]. The CCM a_v is a bit larger than that of the SOM, and the r_v is considerably smaller. The CCM and SOM J_v values are similar, and the r_w and a_w values have qualitatively the same magnitudes and energy dependencies. However, the imaginary strengths, J_w , are quite different. The CCM J_w increases with energy as one would expect as more channels become open. Furthermore, the CCM J_w magnitude is smaller over most of the energy range as one would expect due to the explicit attention to the vibrational channel. Relatively large SOM J_w values in this mass-energy range were reported from this laboratory sometime ago [2], and attributed to the qualitative approximation of known collective vibrators using a simple spherical model.

The CCM leads to significant direct excitation of the yrast 2^+ state, as illustrated in Fig. III-5. In fact, the one-phonon CCM model over-estimates this direct contribution by $\approx 30\%$. This is in contrast to experience at shell closures (e.g., ^{58}Ni [55]), but cadmium is not at a shell closure and thus the simple vibrational model may be less appropriate. It is known that CCM calculated results are diluted when one extends the model to include two-phonon excitations, with results in the present case in very good agreement with the observed inelastic-scattering cross sections of the yrast 2^+ level, as illustrated in Fig. III-5. The calculational time involved with this extended one- and two-phonon CCM is a factor of five or more longer than for the simple one-phonon model. This computational reality made comprehensive re-fitting of the entire elastic-scattering data base with the one- and two-phonon model unattractive. However,

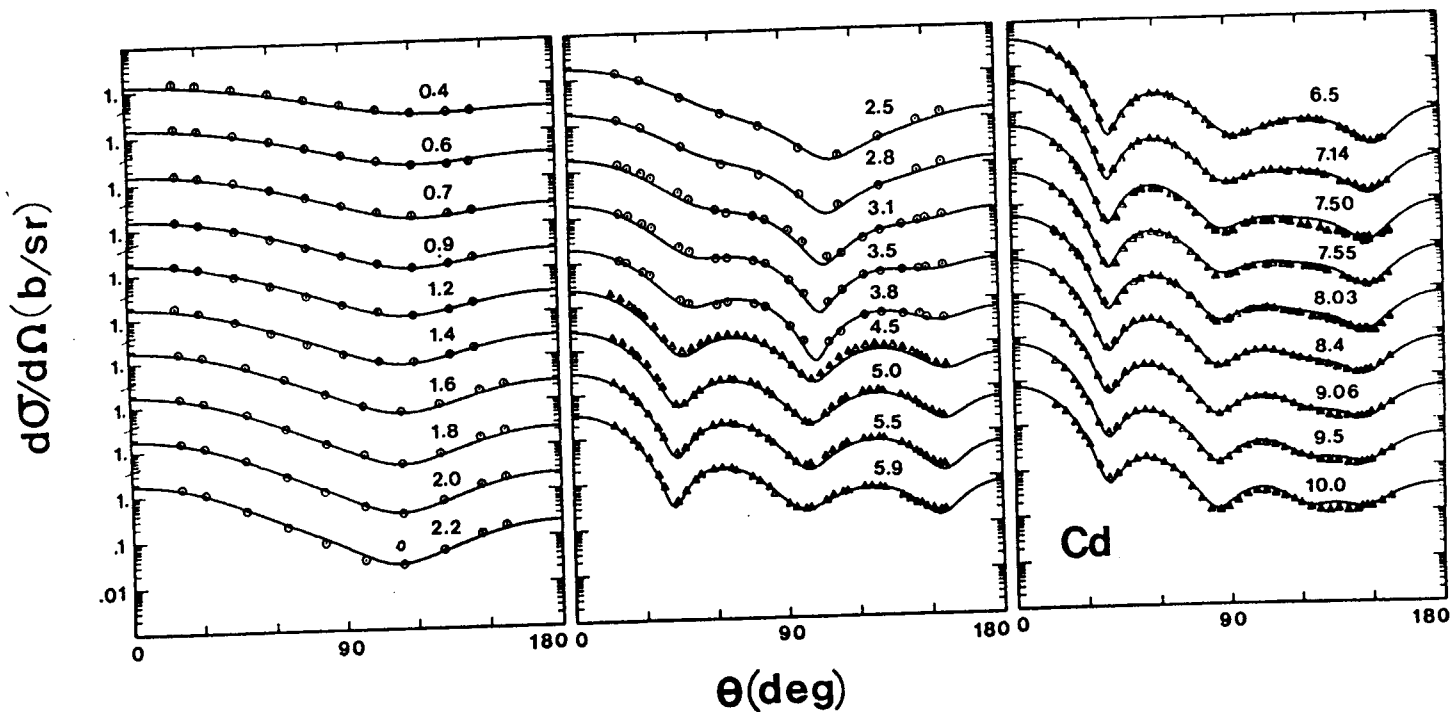


Fig. IV-8. Comparison of measured (symbols) and calculated (curves) differential elastic-scattering cross sections of cadmium. The calculations were made using the CCM, and the notation is identical to that of Fig. IV-1.

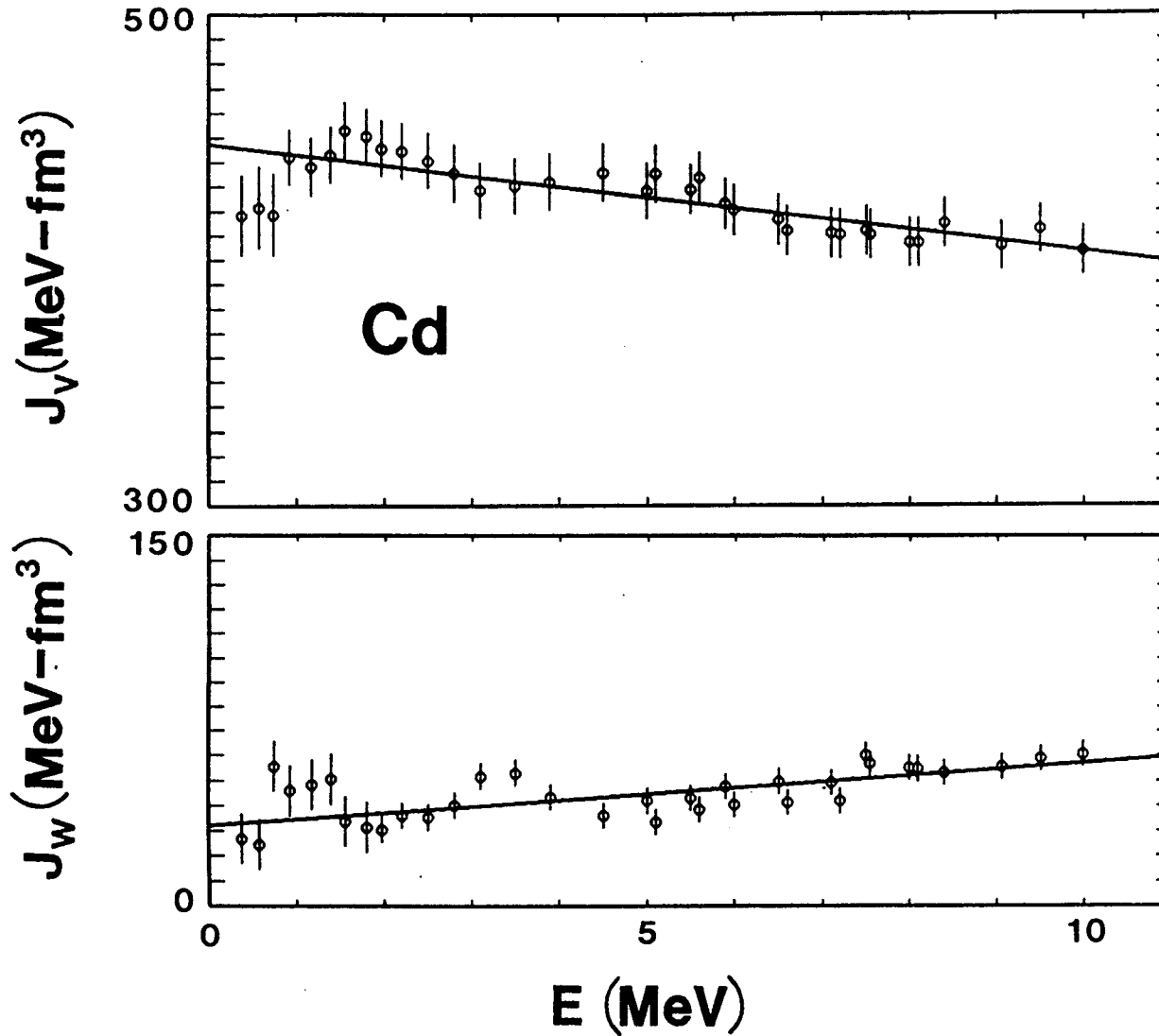


Fig. IV-9. Real, J_v , and imaginary, J_w , CCM potential strengths expressed as volume-integrals-per-nucleon. Symbols indicate the results of the fitting described in the text, and curves the parameterizations of Table IV-5.

Table IV-5. Parameters of the one-phonon CCM potential. The notation is identical to that of Table IV-2. The parameterization is rigorously valid only up to 10 MeV, as discussed in the text.

Real Potential (V)

$$J_v = 447.5 - 4.417 \cdot E$$

$$r_v = 1.2600$$

$$a_v = 0.6669$$

Imaginary Potential (W)

$$J_w = 32.06 + 2.502 \cdot E$$

$$r_w = 1.431 - 0.01006 \cdot E$$

$$a_w = 0.19137 + 0.04439 \cdot E$$

Spin-Orbit Potential (SO)

Identical to that given in Table IV-1.

Deformation, $\beta_2 = 0.175$ (see text for definition)

several tests in the incident-energy range 6 - 8 MeV indicated that the use of the extended model does not substantively alter the one-phonon model parameters of Table IV-5. The effect of the extended model is primarily evident in the inelastic channels. The influence of the two-phonon excitations is also evident in comparison of measured and calculated inelastic-scattering distributions, as illustrated in Fig. IV-10. Generally, the simple one-phonon CCM leads to angular distributions of qualitatively the right shape but of too large a magnitude. The results obtained with the one- and two-phonon CCM are in better agreement with the observations. The calculated differential inelastic-scattering shapes are quite consistent with the measured values, except at very-large scattering angles (i.e., $\geq 150^\circ$). At angles forward of $\approx 90^\circ$ the calculated differential-cross-section magnitudes tend to be slightly larger than the measured values, particularly at the lower energies, but the discrepancies are approximately of the same magnitude as the estimated experimental uncertainties. The theoretical aspects of such comparisons are discussed in ref. [4].

An alternative to the above one- and two-phonon model is the one-phonon model with a reduced β_2 . This avenue was explored, and it was found that essentially the same results could be obtained as with the one- and two-phonon model (Figs. III-5 and IV-10) if β_2 is reduced to $0.150 \pm \approx 7.5\%$. The effect of this change on the σ_t is small and the differential elastic-scattering cross sections are very similar to those obtained with the larger β_2 . The governing factor throughout these considerations is the comparison of measured and calculated inelastic-scattering cross sections. The implications of these alternatives are further discussed below.

V. DISCUSSION AND SUMMARY

An objective of the present work was the provision of neutron data and associated models for applications purposes, particularly for evaluated neutronic data for the fission-product cadmium isotopes. For many applied purposes, the SOM of Table IV-1 should prove a suitable calculational vehicle. It is simple to use, and will, for example, give reasonable transmission coefficients for the prediction of neutron statistical emission spectra, for compound-nucleus formation and subsequent γ -ray emission, etc. However, the SOM remains essentially a local model. Its real potential reflects nuclear structure via the dispersion relationship and thus it is not of a "global" nature. In some isotopic applications of the SOM it may be useful to employ small (e.g. few percent) engineering bias factors obtained, for example, by renormalizing the calculated cross sections to give exact agreement with the experimentally-deduced total cross section. The SOM certainly is inappropriate for treating direct

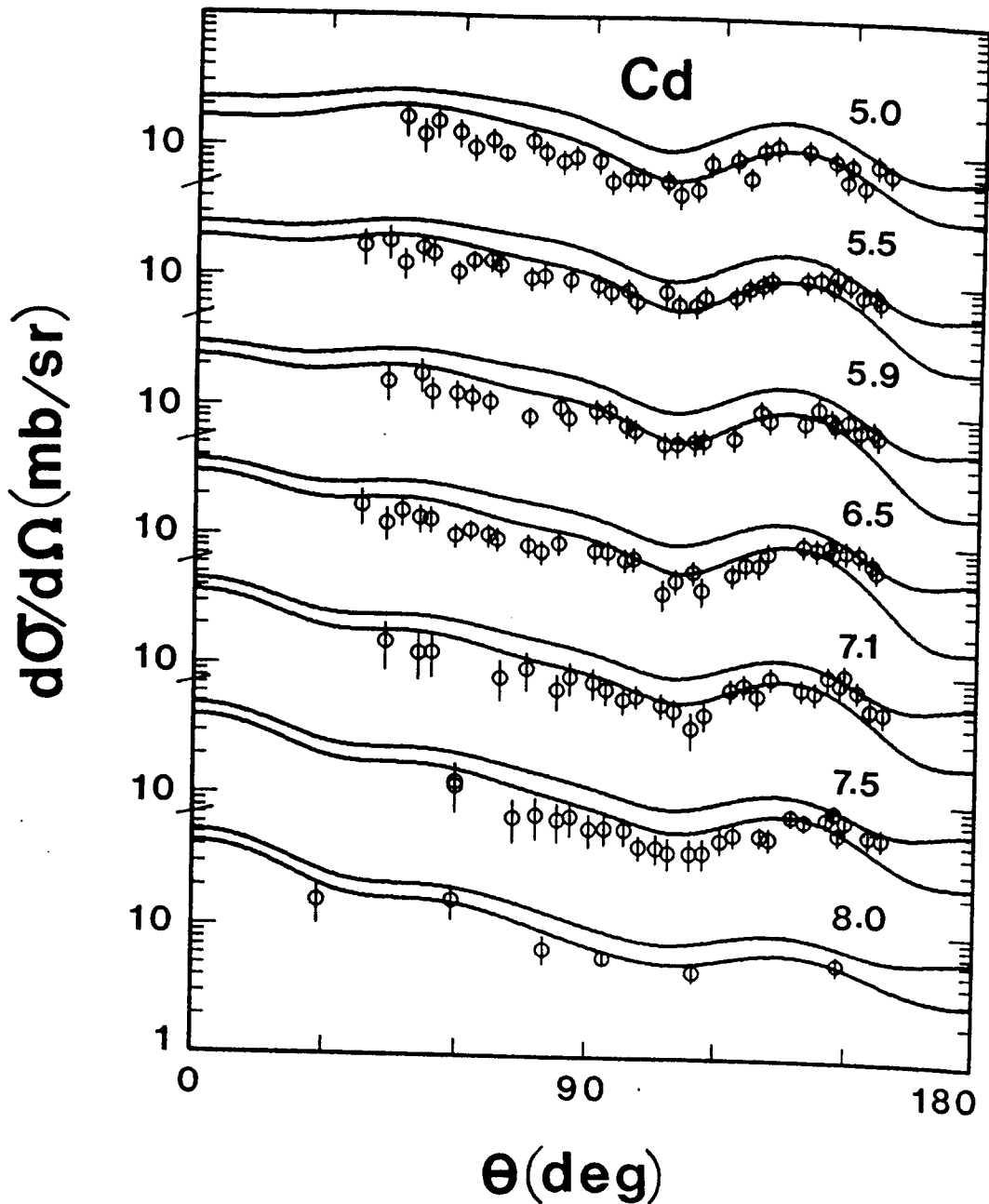


Fig. IV-10. Comparison of measured (symbols) and calculated (curves) differential cross sections for the inelastic-neutron excitation of the yrast 2^+ levels in the cadmium isotopes. In each case, the upper curve corresponds to calculations with the one-phonon CCM, and the lower curve that obtained with the one- and two-phonon CCM. The incident-neutron energies are numerically given in MeV.

reactions due to the collective nature of the cadmium isotopes. This shortcoming is clearly evident in the context of inelastic neutron scattering where, even at relatively low energies, the direct inelastic-scattering cross sections can be of considerable size. The DOM has the advantage of a real potential more nearly of a "global" nature, approaching the general Hartree-Fock behavior and is physically attractive, as outlined below. However, in the spherical formulation used here, it too remains devoid of a capability to handle the direct reactions due to the collective nature of the cadmium isotopes. For those applications sensitive to collective processes, the CCM has an outstanding advantage. These various applied capabilities are being exploited at this laboratory to provide comprehensive evaluated neutronic data files for the cadmium isotopes [5].

The SOM parameterization (Table IV-1) displays conventional characteristics of a spherical model for collective vibrators in the cadmium mass region. The real-potential diffuseness is reasonably conventional, but the real-potential radius is relatively large, as is characteristic of SOM descriptions of strong collective vibrators [57,58]. At low incident energies, the imaginary-potential radius is appreciably larger than the real-potential radius. Such a characteristic has long been observed in low-energy SOM neutron interpretations [59], particularly those giving emphasis to the strength functions. The imaginary diffuseness becomes quit small as $E \rightarrow 0$, again a characteristic that has been widely observed [10,32,55,60,61]. The real-potential strength is of a frequently encountered magnitude, and decreases with energy in an approximately linear manner. In contrast, the imaginary-potential strength is quite large and, contrary to expectations, generally decreases with energy. This is, again, a consequence of using the SOM for interpretations of neutron phenomena in a collective vibrational environment [2,57,58]. The majority of the SOM parameters are energy dependent. These energy dependencies are reasonably valid only within the $0 \rightarrow 10$ MeV range of the present interpretations, and can not continue to very large energies. There is no experimental evidence to define such high-energy behavior, but it is reasonable to expect some asymptotic approach to energy-constant values, excepting the real-potential strength which is expected to continue to fall in a manner consistent with the Hartree-Fock potential. Likewise, the present study to ≈ 10 MeV gives no evidence of a volume absorption, but it is reasonable to expect volume absorption to be significant above $\approx 15 \rightarrow 30$ MeV.

The DOM parameterization (Table IV-3) inherently has the same shortcomings as that of the SOM in that it is a spherical approximation of collective nuclei. Predictably, the DOM and SOM imaginary-potential representations are quite similar. Some of the DOM imaginary-potential parameterizations are quadratic rather than linear, as for the SOM, but that is only a statistical artifact, and the general trends with energy are very similar. The major differences between DOM and SOM representations are in the real

potential where the impact of the dispersion integral is apparent. The real-potential diffuseness of the DOM is somewhat larger than that of the SOM as a narrow surface component of the potential has been removed from the general Saxon-Woods form. For the same reason, the DOM real-potential radius is smaller than that of the SOM, though still larger than expected from "global" systematics (see remarks below). The DOM real-potential strength (the J_{eff} of Eq. IV-4) is considerably less than that of the SOM, by an amount governed by the dispersion integral of Eq. IV-2. The latter reflects structural contributions to the general Hartree-Fock trend. Thus it is the DOM real-potential strength that should be addressed when considering "global" trends. As for the SOM interpretation, the present DOM interpretation is rigorously valid only for $E \leq 10$ MeV

The CCM (Table IV-5) is inherently different from either the SOM or DOM in both physical concept and parameterization. It alone can reasonably account for the direct-reaction aspects of the interaction of neutrons with the collective cadmium isotopes, particularly that facet of the interaction dealing with inelastic neutron scattering. The CCM real-potential radius is considerably smaller than that of the SOM, and more consistent with "global" trends (as discussed below). The CCM real-potential strength is very similar to that of the SOM, the differences probably being statistical artifacts. The CCM-SOM differences are most evident in the imaginary potential. The strength of the latter is considerably less than that of the SOM at lower energies, and increases with energy as one would expect from the opening of additional channels not explicitly addressed in the interpretations. These differences between CCM and SOM representations of collective nuclei have been recognized previously [57,58], and reflect the inappropriate nature of the SOM when treating strong collective vibrators. The parameters of the CCM were obtained using the one-phonon approximation. If one seeks a more accurate representation of the direct-reaction processes (particularly inelastic scattering) more complex coupling (or an adjustment of β_2) should be used. The next step in the hierarchy of coupling is the one- and two-phonon CCM model, at the expense of computational complexity. Like the SOM and DOM, the CCM energy dependence is not defined above ≈ 10 MeV. That will not be possible until some reasonable measured neutron data becomes available to guide the physical interpretations.

As neutron studies and associated interpretations mount up at this laboratory, systematic trends in, particularly, the real SOM potential are emerging. These are best assayed at ≈ 8 MeV where the contribution of the dispersion relation to the model derivations is small, and that is reasonably so for the present cadmium case. At 8 MeV, it has been shown [10,61] that the real SOM potential radius has a mass dependence of the form:

$$r_v = r_0 + r_1/A^{1/3}, \quad (V-1)$$

where $r_0 = 1.154$ fm and $r_1 = 0.407$ fm. This expression is consistent with the low-energy model of Moldauer [59], and implies a cadmium r_v value of 1.2383 fm, considerably less than that obtained with SOM. The comparison is more attractive if made with the present CCM r_v (the difference is 1.71%). Closer agreement should probably not be expected as Eq. V-1 is based upon essentially spherical nuclei and therefore not strictly appropriate for the collective cadmium isotopes. With the form factor of Eq. V-1, it was shown in refs. [10] and [61] (and references cited therein) that the real-potential strength of the SOM at ≈ 8 MeV had a systematic behavior described by

$$J_v = K_0 \cdot [1 - \xi(N-Z)/A] \cdot (r_0 + r_1/A^{1/3})^3, \quad (V-2)$$

where $K_0 = 236.1$ and $\xi = 0.575$ [61] (alternatively, ref. [10] gives 234.1 and 0.53, respectively). These values of ξ are reasonably consistent with that obtained from nucleon-nucleon scattering data (0.48) [62] and (p,n) studies (0.40) [63], and considerably smaller than that obtained with the simple isovector expression $J_0 = J_0 \cdot [1 - \xi(N-Z)/A]$. Applying Eq. V-2 to the cadmium case, one obtains a $J_v = 410$ MeV-fm³, compared to 413 MeV-fm³ from the DOM and 428 MeV-fm³ from the SOM. Thus, Eqs. V-1 and -2, with $a_v \approx 0.65$, remain a reasonable "global" starting point for more specific SOM interpretations, while remaining cognizant of possible collective effects that may distort their reliability.

The nuclear equation of state (EOS) is of continuing fundamental interest, and has implications on astrophysical considerations [64]. An often cited observable supporting EOS concepts is the real optical potential taken over a wide energy range extending from perhaps ≈ -100 MeV to +200 MeV. The proton potential is frequently used as it is the only such potential based upon such a wide energy range of measured data. However, the low-energy behavior is obscured by coulomb effects, and it is known that the energy dependence of the real proton OM potential is anomalous near the Fermi energy [65,66]. Therefore, in considering the behavior of the potential in a wide energy scope the "critical" region $|E| \leq E_{crit}$ is avoided, where E_{crit} is 20 - 30 MeV. The general behavior of the real proton optical potential has been examined by a number of authors. For example, Bauer et al. [67] describe the real part of the proton OM potential, V , with the expression

$$V = 52.4 - 0.37 \cdot E + 0.0007 \cdot E^2 + 24 \frac{N-Z}{A} + 0.4 \frac{Z}{A^{1/3}}. \quad (V-3)$$

The equivalent real part of the neutron OM potential would be

$$V = 52.4 - 0.37 \cdot E + 0.0007 \cdot E^2 - 24 \frac{N-Z}{A}, \quad (V-4)$$

where the Coulomb term is no longer applicable and the sign of the isovector term is reversed. Eq. V-4 should be comparable with the J_v of the DOM (Table IV-4) of the present work as in that case the majority of the dispersion contributions to the real potential have been removed. Using Eq. V-4, and accounting for the differences between the geometries of ref. [67] and those of the present work, one obtains a $J_v(E \rightarrow 0) = 431.89 \text{ MeV} \cdot \text{fm}^3$. This differs from the J_v of the present DOM by only 1.36%. This is remarkable agreement, particularly in view of the fact that small perturbations due to collective effects and ΔJ_{v0} of Eq. IV-3 were ignored, and suggests that the isovector strength of Eq. V-4 is reasonably correct. In the context of Eq. V-2, it implies $\xi \approx 0.48$, which is consistent with the value obtained from the systematic studies of refs. [10] and [61], but not with some "global" SOMs [31]. However, the dJ_v/dE implied Eq. V-4 (and associated geometries of ref. [67]) is approximately twice that of the present DOM. This is a reflection of the well-known anomalous behavior of the optical potential in the region of the Fermi Surface, which is in part due to the dispersion integral (Eq. IV-2), as pointed out by Mahaux and Ngo [53]. These dispersive effects have been removed in the present DOM interpretation to the extent that the underlying assumptions made in the interpretation are valid.

Brown et al. [68] have treated the region near the Fermi Surface using a dynamic theory of vibrations. From their considerations, the reduced mass, m^* , near the Fermi Surface, is given by [67,68]

$$\frac{m^*}{m} = 0.64 + 0.36 \cdot [1 + |E - E_F| / (2h\omega_0)]^{-2}. \quad (V-5)$$

Concurrently, $dV/dE = 1 - \frac{m^*}{m}$. Taking $h\omega_0 = 41/A^{1/3}$ [68], Eq. V-5 leads to $(dV/dE)_{E \rightarrow 0} = 0.1922$ as compared to the values of 0.1571 (DOM) and 0.3700 (SOM) following from the present interpretations. The difference between the result following from Eq. V-5 and the DOM is $\approx 23\%$, which is within the estimated uncertainty ($\approx 30\%$) of the experimentally-deduced value. The agreement is less suitable for the SOM result, as is to be expected since the dispersive effects have not been removed.

The present CCM and experimental results, particularly those dealing with inelastic neutron scattering, imply β_2 values significantly smaller than those deduced from electro-magnetic

measurements. Quantitative comparisons should employ the deformation length, $\delta_i = R_i \cdot \beta_i$ [69]. Expressed in this form, $\delta_{em} = 1.014$, where the β_{em} is taken from ref. [4] with the associated $R = 1.2 \cdot A^{1/3}$ fm.

For comparison, the present $\delta_{nn} = 0.9110 \begin{bmatrix} 0.9793 \\ 0.8427 \end{bmatrix}$, where the range in values reflects estimated uncertainties in β_{nn} alone. In addition, there may be uncertainties due to R , which are difficult to determine accurately as it is strongly correlated with the real strength, V . A number of parameter studies failed to display any strong dependence of δ_{nn} on the imaginary radius, r_w . Clearly, $\beta_{nn} < \beta_{em}$ in the present cadmium case, in contrast to the theoretical estimates of Madsen et al. [70], which predict $\beta_{em} < \beta_{nn} < \beta_{pp}$ reflecting isovector effects,

and as experienced dealing with ^{58}Ni [55,71]. The theoretical estimates are made for nuclei with closed neutron or proton shells, and not necessarily applicable to targets off the closed shells, as for the present cadmium case. Similar discrepancies have been observed when dealing with permanently deformed nuclei [72], and have been attributed to the interaction of the incident particle with the collective surface of the target which, in the present case is neutron rich. Similar estimates of such effects for collective vibrators have apparently not been made. Another contributing factor may be the non-zero range of a realistic interaction [70], not treated by the theory. Theoretical estimates tend to be essentially perturbation calculations, thus comparisons with the results of DWBA calculations are perhaps more appropriate. The latter lead to larger radii than coupled channel calculations [71], and thus it may be reasonable to consider the SOM radius in determining δ_{nn} . With that approach, the present results lead to a δ_{nn} that, within uncertainties, is consistent with the δ_{em} deduced from ref. [4]. Finally, it should be noted that experimental studies of similar vibrational nuclei are in progress at this laboratory, the results of which should, hopefully, illuminate the problem. Concurrently, theoretical considerations are in progress, free of many of the limitations of the simple vibrational model used in the above CCM interpretations.

ACKNOWLEDGEMENTS

The authors are very much indebted to Dr. R. D. Lawson for his consultation and advice throughout this work.

REFERENCES

1. Evaluated Nuclear Data File/B, Version VI (ENDF/B-VI), available from the National Nuclear Data Center, Brookhaven National Laboratory.
2. A. B. Smith, P. T. Guenther and J. F. Whalen, Nucl. Phys. A415 1 (1984).
3. See:- D. de Frenne, E. Jacobs and M. Verboven, Nucl. Data Sheets 53 73 (1988); R. L. Haese, F. E. Bertrand, B. Harmatz and M. J. Marten, Nucl. Data Sheets 37 289 (1982); P. de Gelder, E. Jacobs and D. de Frenne, Nucl. Data Sheets 38 545 (1983); J. Blachot and F. Haas, Nucl. Data Sheets 60 889 (1990); D. de Frenne, E. Jacobs and M. Berboven, Nucl. Data Sheets 57 443 (1989); J. Blachot, Nucl. Data Sheets 59 729 (1990); J. Blachot and G. Marguier, Nucl. Data Sheets 60 139 (1990); and J. Blachot and G. Marguier, Nucl. Data Sheets 59 333 (1990).
4. R. D. Lawson and A. B. Smith, Argonne National Laboratory Report, to be published.
5. A. B. Smith, J. W. Meadows and R. J. Howerton, Evaluated Neutronic Data Files for the Cadmium Isotopes, ANL/NDM Report, to be published.
6. L. Cranberg and J. Levin, Proc. Inter. Conf. on Peaceful Uses of Atomic Energy, IAEA Press, Geneva (1955).
7. A. Smith, P. Guenther, R. Larsen, C. Nelson, P. Walker, and J. Whalen, Nucl. Instr. and Methods 50 277 (1967)
8. A. Smith, P. Guenther and R. Sjoblom, Nucl. Instr. and Methods 140 3907 (1977)
9. P. T. Guenther, The scattering of fast neutrons from the even isotopes of tungsten, University of Illinois Thesis (1977)
10. S. Chiba, P. T. Guenther, R. D. Lawson and A. B. Smith, Phys. Rev. C42 2487 (1990).
11. P. T. Guenther, A. B. Smith and J. F. Whalen, Phys. Rev. C12 1797 (1976); see also ref. [32].
12. A. B. Smith, P. T. Guenther and R. D. Lawson, The neutron interaction with calcium, and the mean nuclear field, Argonne National Laboratory Report, in press.
13. J. W. Meadows and D. L. Smith, Argonne National Laboratory Report ANL/NDM-53 (1980).

14. 1983 Nuclear Standards File (IAEA Tech. Report 227), editors H. Conde, A. Smith and A. Lorenz, IAEA Press, Vienna (1983).
15. A. B. Smith, P. T. Guenther and R. D. McKnight, Proc. Conf. on Nucl. Data for Science and Technology, editor K. H. Boeckhoff (Reidel, Dordrecht, Holland, 1982) p. 39.
16. A. B. Smith and P. T. Guenther, Argonne National Laboratory Report ANL/NDM-72 (1982).
17. A. B. Smith, unpublished memorandum, available from the author (1991).
18. W. Vonach and A. B. Smith, Nucl. Phys. 78 389 (1966).
19. M. Walt and J. Beyster, Phys. Rev. 98 667 (1955).
20. R. Wilenzick, K. Seth, P. Bevington and H. Lewis, Nucl. Phys. 62 511 (1965).
21. R. Becker, W. Guindon and G. Smith, Nucl. Phys. 89 154 (1966).
22. S. Snowdon and W. Whitehead, Phys. Rev. 94 1267 (1954).
23. B. Holmqvist and T. Wiedling, Aktiebolaget Atomenergi Report AE-430 (1971).
24. M. Etemand, Aktiebolaget Atomenergi Report AE-482 (1973).
25. P. A. Moldauer, private communication (1982), as modified by S. Chiba (1989).
26. W. Hauser and H. Feshbach, Phys. Rev. 87 362 (1952).
27. P. A. Moldauer, Nucl. Phys. A344 185 (1980).
28. A. Gilbert and A. Cameron, Can. J. Phys. 43 1446 (1965).
29. P. E. Hodgson, Nuclear Reactions and Nuclear Structure (Oxford, Clarendon, 1971).
30. W. Poenitz and J. Whalen, Argonne National Laboratory Report, ANL/NDM-80 (1983).
31. R. L. Walter and P. P. Guss, Proc. Conf. on Nucl. Data for Basic and Applied Science, editors P. Young et al. (New York, Gordon and Breach, 1986) vol. 2, p. 1079.
32. For example see S. Chiba, P. T. Guenther, A. B. Smith, M. Sugimoto and R. D. Lawson, Phys. Rev. C45 1260 (1992).

33. A. B. Smith, Argonne National Laboratory Report, to be published.
34. M. Khaletskij, Doklady Akademii Naak SSSR 113 305 (1956).
35. K. Tsukada and T. Lee, Nucl. Phys. 83 274 (1966).
36. S. Snowdon and W. Whitehead, Phys. Rev. 94 1267 (1954).
37. D. Foster and D. Glasgow, Phys. Rev. C3 576 (1971).
38. A. Bratenahl, J. Peterson and J. Stoering, Phys. Rev. 110 927 (1958).
39. N. Nereson and S. Darden, Phys. Rev. 94 1678 (1954).
40. C. Johnson, H. Willard, J. Blair and J. Kington, Oak Ridge National Laboratory Report, ORNL-1365 (1953).
41. M. Walt and J. Beyster, Phys. Rev. 98 677 (1955).
42. L. Green and J. Mitchell, Proc. Conf. on Nucl. Data for Sci. and Technology, CONF-710301 (1971) vol. 1, p. 325
43. J. Coon, E. Graves and H. Barschall, Phys. Rev. 88 562 (1952).
44. J. Peterson, A. Bratenahl and J. Stoering, Phys. Rev. 120 521 (1960).
45. T. Haugsnes, J. Dissertation Abstracts/B 28 3835 (1968).
46. P. H. Bowen, J. Scanlon, G. Stafford and J. Thresher, Nucl. Phys. 22 640 (1961).
47. M. Walt, R. Becker, A. Okazaki and R. Fields, Phys. Rev. 89 127 (1953).
48. G. McCallum, G. Mani and A. T. G. Ferguson, Nucl. Phys. 16 313 (1960).
49. A. Taylor and E. Wood, J. Phil. Mag. 44 95 (1953).
50. R. Maggi Ortega, INIS-MF International Information System 1743 (1975), IAEA Vienna.
- 51 S. F. Mughabghab, M. Divadeenam and N. E. Holden, Neutron Cross Sections (Academic, New York, 1981).
52. G. R. Satchler Direct Nuclear Reactions (Clarendon Press, Oxford, 1983).

53. C. Mahaux and H. Ngo, Nucl. Phys. A378 205 (1982); also Phys. Lett. 100B 285 (1981).
54. S. Raman, C. H. Malarkey, W. T. Miller, C. W. Nestor Jr. and P. H. Stelson, Atom. Data and Nucl. Data Tables 36 1 (1987).
55. A. Smith, P. Guenther, J. Whalen and S. Chiba, J. Phys. G18 629 (1992).
56. ANLECIS, A Neutron Coupled-Channels Code, P. A. Moldauer (1982); Adapted from ECIS-79, J. Raynal, NEA Data Bank Notes (1979).
57. R. D. Lawson, A. B. Smith and M. Sugimoto, Bull. Am. Phys. Soc. 32 No.-1, 32 (1987)
58. A. B. Smith, Memorandum (1991), unpublished.
59. P. A. Moldauer, Nucl. Phys. 47 65 (1963).
60. A. B. Smith, P. T. Guenther and R. D. Lawson, Nucl. Phys. A483 50 (1988).
61. A. B. Smith and P. T. Guenther, Argonne National Laboratory Report ANL/NDM-125 (1992).
62. G. W. Greenlees, W. Makofske and G. J. Pyle, Phys. Rev. C1 1145 (1970).
63. C. J. Batty, E. Friedman and G. W. Greenlees, Nucl. Phys. A127 368 (1969).
64. L. P. Csernai, G. Fai, C. Gale and E. Osnes, Phys. Rev. C46 736 (1992).
65. G. E. Brown, J. H. Gunn and P. Gould, Nucl. Phys. 46 598 (1963).
66. C. J. Batty and G. W. Greenlees, Nucl. Phys. A133 673 (1969).
67. M. Bauer, E. Hernandez-Saldana, P. E. Hodgson and J. Quintanilla, J. Phys. G8 525 (1982).
68. G. E. Brown, J. S. Dehesa and J. Speth, Nucl. Phys. A330 290 (1979).
69. J. S. Blair Direct Interactions and Nuclear Reaction Mechanisms editors E. Clementel and C. Villi (Gordon and Breach, New York, 1963) p. 669.
70. V. A. Madsen, V. R. Brown and J. D. Anderson, Phys. Rev. C12 1205 (1975).

71. Y. Yamanouti, J. Rapaport, S. M. Grimes, V. Kulkarni, R. W. Finlay, D. Bainum, P. Grabmayr and G. Randers-Pehrson, Proc. Conf. on Nuclear Cross Sections and Technology, editors J. Fowler, C. Johnson and C. Bowman, NBS Spec. Pub. 594 (1980) p. 146.
72. D. L. Hendrie, Phys. Rev. Lett. 31 478 (1973).